

**Objective Identification, Typing and Tracking of the Complete Life-Cycles of Cyclonic Features at High Spatial Resolution**

Journal:	<i>Meteorological Applications</i>
Manuscript ID:	MET-09-0042.R3
Wiley - Manuscript type:	Research Article
Date Submitted by the Author:	
Complete List of Authors:	Hewson, Timothy; ECMWF, Operations Titley, Helen; Met Office, NWP
Keywords:	Cyclone, Windstorm, Frontal wave, Vorticity, Objective front, Ensemble, Forecasting



# **Objective Identification, Typing and Tracking of the Complete Life-Cycles of Cyclonic Features at High Spatial Resolution**

Tim D. Hewson, ECMWF, Shinfield Park, Reading, and  
Helen A. Titley, Met Office, Exeter, UK

## **Abstract**

Synoptic-scale cyclonic features provide an inescapable focal point for operational forecasting, whilst the merits of tracking such features are increasingly being recognised in the climate change field. Close association with adverse and extreme weather is the main motivator. Here we develop a new and highly sophisticated set of techniques to detect, classify and track the full range.

A revised conceptual model of cyclone development provided the initial framework, ensuring a solid bond with forecasting practice, whilst also connecting closely to baroclinic life-cycle concepts. Building on this, we detect cyclones using a hybrid of geopotential minimum / vorticity maximum techniques, whilst incorporating important extensions to ensure that vorticity can be used at high resolution (~50 km) and that features on fronts take priority.

To track the features across time, at intervals of 12 h or less, we use feature attributes in the association process. Additionally, an upper-tropospheric steering wind is employed to estimate future and past positions. This facilitates 'half-time tracking', a new approach that has clear-cut advantages over 'full-time tracking' employed elsewhere.

In detection tests, comparing with subjectively-drawn charts, the feature hit rate was 84%, and the false alarm ratio 17%, whilst in a simple tracking test the association failure rate was just 2%. These values compare very favourably with previous studies.

One key application is discussed. This involves processing ensemble output to provide wide-ranging real-time products tailor-made to forecaster's needs. Products include track-following plume diagrams, for various cyclone attributes, and storm-track strike probability plots for different thresholds of severity.

**Keywords:** Cyclone, Windstorm, Frontal wave, Vorticity, Objective front, Ensemble, Forecasting, Post-processed Product

## **1. Introduction**

Automatic detection of cyclonic features, in model fields, has historically relied on forms of gridpoint searching to identify either mean sea level pressure minima or low-level vorticity maxima (e.g. see Hoskins and Hodges, 2002). Hewson (1997) took a rather different approach, for the extra-tropics, by focusing on features that develop on fronts, specifically frontal wave cyclones. This technique has its roots in synoptic practice where frontal waves have long been identified on charts, and recognized as portents of bad weather. The same paper also illustrated how these new algorithms could extend a cyclone life cycle back in time. More recently, Hewson (2009a) extended this conceptual life cycle even further back, to the earliest imaginable point, introducing the term

1  
2 'diminutive wave' to represent, primarily, this incipient stage. In parallel, the frontal wave and  
3 diminutive wave stages were also appended to the start of the familiar Shapiro and Keyser (1990)  
4 conceptual model, as illustrated in Figure 1. This depicts the idealized life-cycles of two cyclones,  
5 one starting out on a cold front (top, from Hewson, 2009a) the other on a warm front (bottom,  
6 new). For completeness a 'decay' stage (7) has now been added to the end; the transition from stage  
7 6 to stage 7 being characterized by filling and frontolysis.  
8  
9

10 In conjunction with the Hewson (2009a) study, the range of objective techniques was expanded,  
11 into a new and all-embracing framework, to enable all the different stages of this revised  
12 conceptual model to be identified (recognizing three feature types, labeled at the bottom of Figure  
13 1). The current paper broadly focuses on this framework, and has three related aims:  
14

- 15 • **detection** - to detail the new objective identification methodology
  - 16 • **tracking** - to describe the coupling to a new feature tracking algorithm
  - 17 • **applications** - to discuss and illustrate current applications
- 18  
19  
20

21 In this introduction we deal briefly with these three topics, and then in subsequent sections discuss  
22 them in detail. Areas where we believe our new approach has a significant advantage will be  
23 highlighted.  
24  
25

26 The **detection** method is vastly different from anything previously used in this field, and for this  
27 reason will be thoroughly documented. In essence it is a hybrid of the vorticity maximum and  
28 pressure minimum ('univariate') detection techniques, though with important extensions to bring in  
29 fronts and use a new, related, vorticity partition. This hybrid approach follows in the spirit of König  
30 *et al* (1993) who allowed the early part of a cyclone's evolution to sometimes be represented as a  
31 low level vorticity maximum, although they made no reference to fronts or vorticity partitions, and  
32 had only 900 km resolution data at their disposal. To the authors' knowledge König *et al*'s  
33 technique is the only other true extra-tropical 'hybrid technique' in the literature. For tropical  
34 cyclone tracking, hybrid techniques have been more common - e.g. Kleppek *et al* (2008).  
35  
36  
37

38 In our hybrid approach we use a novel diagnostic-graphical method to pinpoint each feature. This  
39 involves two feature-specific steps, followed by two post-processing steps applied to all features  
40 collectively. The first feature-specific step is to compute a number of diagnostics on a particular  
41 atmospheric level from raw, gridded numerical model data. The second is to then pinpoint each  
42 feature using graphical devices such as standard contouring and colour-filling applied to these  
43 diagnostic fields. Thereafter, the post-processing steps deal with overlapping definitions (e.g. a  
44 frontal wave tip may also be at a low pressure centre), and other aspects. Whilst diagnostic  
45 variables defined in Hewson (1997) cater for the frontal wave feature (stages 2 to 5) on Figure 1,  
46 new variables introduced here deal specifically with diminutive waves (stage 1) and barotropic low  
47 pressure centres (stages 6 and 7), to complete the set.  
48  
49  
50

51 The new hybrid detection techniques are more involved than previous univariate methods, but have  
52 many benefits:  
53

- 54 1) They are better suited to dealing with the rich variety of cyclone behaviour seen in high  
55 resolution models
  - 56 2) They are strongly connected to operational synoptic and forecasting practice
  - 57 3) The influence of land-sea contrasts, sea surface temperature gradient and orography is  
58 better elucidated
  - 59 4) Life-cycles are in general longer, notably for small-scale cyclonic windstorms
- 60

1  
2 Expanding on point 1, many studies continue to use data with horizontal resolution in the range 100  
3 to 500 km - e.g. in Bengtsson *et al* (2009) and Froude (2009) data are upscaled to ~450 km  
4 resolution for detection and tracking purposes. This is because higher resolution data can present  
5 problems, as they and other authors have recognized. Here we can successfully use data with a  
6 resolution of order 50 km. Benefits 2, 3 and 4 then arise naturally out of being able to directly  
7 utilize data at this higher resolution.  
8  
9

10 The techniques we describe have been applied to operational model output for some time. Feature  
11 identification has also been coupled with 'attribute extraction' to form a cyclone database (an early  
12 version is described in Hewson 1998b). This database contains, for each cyclonic feature, a wide  
13 range of diagnostic quantities (such as type, pressure minimum, thickness, maximum wind within  
14 the circulation, quantified quasi-geostrophic forcing from different levels) which in turn have gone  
15 on to be used for other purposes. For example Hewson (2002) used them to diagnose systematic  
16 errors in model forecasts of cyclonic features; Plant *et al* (2003) and Gray and Dacre (2006) to look  
17 at an extended 'Petterssen typing' for North Atlantic cyclones (see Petterssen and Smebye, 1971  
18 and Deveson *et al*, 2002) and Bracegirdle and Gray (2007) to study polar lows. Latterly, Dacre and  
19 Gray (2009) have looked more closely at the evolutionary characteristics of these objective  
20 cyclonic features.  
21  
22  
23  
24

25 Regarding the second topic, *tracking*, it should be noted that both Gray and Dacre (2006) and  
26 Dacre and Gray (2009) used a 'compound' tracking system, that consisted of taking features  
27 identified with the methods in this paper and its forerunners, and following them using Hodges'  
28 (1995) tracker. One disadvantage of this approach, highlighted by Gray and Dacre (2006), was that  
29 ~12% of all features were apparently tracked in the wrong direction (i.e. mis-associated in a  
30 consistent fashion). It was partly for this reason that a new tracking algorithm, specifically tailored  
31 to use the features identified here, was developed. It was felt particularly important to introduce  
32 into it a means of estimating feature movement; this is missing from Hodges' approach and seems  
33 to have been the main reason for the above problem. A second reason for developing the new  
34 algorithm was to successfully track *all* the cyclonic features detected, including those situated on  
35 thermally weak fronts, and without a much more sophisticated means of associating features  
36 between consecutive times this would have been impossible. For Gray and Dacre (2006) and Dacre  
37 and Gray (2009) this was much less of an issue, because neither study incorporated features  
38 situated on weak fronts. An early version of our tracking algorithm was briefly described in Watkin  
39 (now Titley) and Hewson (2006).  
40  
41  
42

43 Note also that considerable effort has gone into trying to ensure that we track not just the modal  
44 cyclones, but also all types of cyclonic windstorm. Without special attention some of these  
45 windstorm systems would have been accidentally discarded, because the behavioural characteristics  
46 that they commonly possess, which have to be recognized within the tracking process, can be  
47 several standard deviations from the norm. Very rapid translation, just prior to sudden deepening, is  
48 one such trait. Such aspects will be discussed further in the tracking section.  
49  
50

51 New techniques were originally researched for a multiplicity of reasons. One was to develop  
52 automated products for operational forecasting; it would appear from published literature that this  
53 was a new goal. Thus an *applications* section has been incorporated into this paper, which we hope  
54 will vividly demonstrate the power of the new methodology. It shows how operational ensemble  
55 data are post-processed in real-time to provide feature-related output in many different formats for  
56 forecasters.  
57  
58

59 The extent to which forecasters accept and utilise output is believed to provide the acid test for any  
60 feature detection and tracking algorithm. In fact it seems to be very unusual for a published method

1  
2 to be put to such a test, so this represents another novel aspect of this study. The requirements for  
3 operations are very demanding. In short feature detection needs to be accurate, needs to replicate  
4 forecasting practice, and needs to make full use of the operational models' resolution. Tracking  
5 must keep false associations to a minimum, with the more extreme cyclones tracked correctly all of  
6 the time. Finally, products must be timely and reliable. This last requirement has forced us to work  
7 with a data time interval of 12 h, whereas other studies on average use 6h. This has meant that  
8 tracking the many features that are detected at high spatial resolution is even more challenging.  
9 However the ultimate reward of addressing this constraint is that when higher temporal resolution  
10 data can be processed, in research for example, then reliability should be greater still.  
11  
12

13  
14 Whilst the geographical focal point has from the outset been the extra-tropics, our hybrid approach  
15 has also proved successful in identifying and tracking tropical cyclones, and where appropriate  
16 following these through extra-tropical transition; an example appears within the applications  
17 section. Our techniques can thus be applied to cyclonic features right across the globe.  
18  
19

20 To set the scene for the following discussion, Figure 2a, adapted from a figure in Hewson (2009a),  
21 shows a snapshot, from a model forecast, of fronts and cyclonic features objectively identified  
22 using the techniques to be described below, together with a depiction of the tracks of these features,  
23 at 12 h intervals. Note how the features and their synoptic evolution often match up well with the  
24 conceptual model in Figure 1, or a portion thereof (diminutive wave → frontal wave → barotropic  
25 low = green → orange → black). This is typical; see Table 2 in Hewson (2009a) for supporting  
26 evidence. Note also how the tracks are smooth and continuous.  
27  
28

29 The paper layout is as follows. Topic area 1, *detection*, is covered in Sections 2-5. In Section 2 the  
30 graphical processing rationale is revisited, before listing the full diagnostic set that provides input to  
31 this. In Section 3 we discuss in more detail, with examples, the diagnostics used for diminutive  
32 waves and (barotropic) low centres. The important post-processing steps are discussed in Section 4;  
33 the term 'barotropic low' relates to these and is also discussed (in section 4.2). Section 5 then  
34 illustrates the correspondence between features identified objectively, and those plotted on  
35 operational charts, to assess the extent to which we can mirror synoptic practice. Topic area 2,  
36 *tracking*, is covered in Section 6, whilst topic area 3, current *applications*, is dealt with in Section  
37 7. The summary, which also lists potential future applications, appears in Section 8.  
38  
39  
40  
41

## 42 2. Graphical processing

### 43 2.1) Rationale

44  
45  
46  
47 As the graphical processing of diagnostics intrinsic to this study differs greatly from strategies  
48 adopted previously there is a need to describe at the outset how this works. To set the scene for  
49 diagnostic selection the general rationale will first be discussed, with the diagnostics themselves  
50 introduced after that.  
51  
52

53 Described as graphical entities, most meteorological features are either curved line segments (e.g.  
54 fronts) or points (e.g. low centres). Sections 2.2 and 2.3 show how simple graphical devices are  
55 used to locate such phenomena, and also how point detection constitutes a simple extension of line  
56 segment detection. These techniques were first touched on in Hewson (1997), with line segment  
57 detection discussed at length in Hewson (1998a).  
58  
59  
60

## 2.2) Line segments

Curved line segments are created (on a blank background) by first plotting zero contours of a particular ‘locating’ diagnostic (Figure 3a) and then erasing portions of these contours (Figure 3c). The erasing proceeds by representing each of one or more ‘masking’ diagnostics as a two-colour colour-fill overlay, using the original background colour to erase and transparent to retain (Figure 3b). The colour boundary value is a ‘masking threshold’. Thresholds are established previously for each diagnostic, with the typical aim of making final output correspond as much as possible to an equivalent manually produced chart, though values can also be adjusted according to purpose. For example in order to also plot weak fronts less stringent thresholds would be used. As well as fronts, easterly wave axes and jet stream cores also fall into the ‘line segment’ category; methods have recently been developed for identifying these features too (see Berry et al, 2007).

## 2.3) Points

Points are represented as the intersections of two zero-contour plots, of two ‘locating’ diagnostics (Figures 3a and 3d). The contour plots are first produced separately, in black on a white background. One is then converted to a graphical overlay, making black transparent (Figure 3e). Overlaying then allows contour intersection points to show through, as small pixel clusters (Figure 3f). Depending on the contouring algorithm, one plot may require more than the minimum contour width to be set, to prevent pixels from near-orthogonal diagonal crossing contours from coincidentally not overlapping. Subsequent post-processing simply converts each pixel group into a single centre-of-gravity point. As with line segment plotting, other diagnostics can be used to mask out certain regions before overlaying contours (Figures 3b and 3c) or after (Figures 3g and 3h). The order of mask application generally has no bearing on the final outcome, though it can influence processing speed. For this new feature detection process we recommend a new name: ‘the intersecting contours method’.

Whilst implementation of the above methodology requires some programming effort, the reward for time invested is a powerful and versatile identification framework, which has numerous possibilities for extension (such as colouring using other variables; see Hewson, 1998a).

## 2.4) Diagnostic list

It will be apparent from the preceding discussion that devising appropriate diagnostics is the key to successfully identifying the requisite cyclonic features. Table I defines the full diagnostic set for each of the three cyclone types, with symbol meaning as follows:

$\nabla$	2-D pseudo-horizontal gradient operator
$(s,n)$	local Cartesian co-ordinates
$\hat{s}_{\text{front}}$	5-point mean axis for defining front-relative local co-ordinates
$\hat{s}_{\text{low}}$	5-point mean axis for defining geopotential height-relative local co-ordinates
$\mathbf{V}$	horizontal wind velocity
$u,v$	horizontal wind components
$\mathbf{V}_G$	geostrophic wind velocity
$V_{Gs}$	geostrophic wind velocity component (resolved into ‘s’ direction)
$\theta$	potential temperature
$\theta_w$	wet-bulb potential temperature
$m$	fractional number of gridlengths (positive)
$\chi$	gridlength (positive)
$\phi_{1000}$	geopotential height of the 1000hPa surface

The ‘frontal wave’ diagnostic set is a slight adaptation of the set described in Hewson (1997). The ‘diminutive frontal wave’ and ‘barotropic low’ sets are new, and are discussed here in detail in Section 3.

For each set the left hand column provides a description of the feature, defines the level at which diagnostics are computed, and illustrates the local co-ordinate system used in computations. The second column provides a label for each diagnostic, and indicates whether these are for locating or masking purposes. The third column describes each diagnostic. The fourth column then provides the equations and inequalities, which collectively form a mathematical representation of the description in column 1. The final column provides threshold values for the inequalities, split into two where necessary to distinguish between features on thermally weak fronts and on standard fronts; the more stringent (higher) thresholds are naturally for the standard fronts. In total we identify five classes of cyclone; barotropic lows, plus two types of frontal wave (standard and weak), plus two types of diminutive wave (standard and weak).

There is evidently a need to calculate all diagnostics at *every* grid point, including those that are ‘front-relative’. This is achieved by first computing, at every grid point, a notional, local, front-normal unit axis  $\hat{s}_{\text{front}}$  (column 1, Table I), using the 5-point mean axis method of Hewson (1998a). This provides local front-relative co-ordinates  $(s,n)$  because  $s$  is simply parallel to  $\hat{s}_{\text{front}}$ . ‘Front-relative’ diagnostics can then be computed across the domain, even in areas remote from fronts; an example is provided later, on Figure 4. In effect, we are providing an accurate approximation to frontal orientation prior to computing where the fronts themselves actually are, meaning that the front-locating process is partly iterative (see Hewson, 1998a). An alternative way of defining  $\hat{s}_{\text{front}}$  would be via the gradient of the front locating diagnostic itself (i.e.  $\nabla$  of DL1 or WL1 on Table I). In tests however this approach provided no clear benefit.

Many of the diminutive wave diagnostics relate directly to the vorticity partition introduced in Hewson (2009a), wherein the full vorticity ( $\zeta$ ) is decomposed into the vorticity of the front-parallel wind, namely the ‘frontal vorticity’ ( $\zeta_{fr}$ ) and the vorticity of the cross-front wind, namely the ‘disturbance vorticity’ ( $\zeta_{di}$ ):

$$\zeta = \zeta_{fr} + \zeta_{di} \tag{1}$$

$$\text{where } \zeta_{fr} = \frac{\partial \mathcal{V}_n}{\partial s} \quad \text{and} \quad \zeta_{di} = -\frac{\partial \mathcal{V}_s}{\partial n} \tag{2}$$

Note that the word ‘disturbance’ as used here is a convenient shorthand reference to ‘cyclonic disturbance’. For supporting information regarding methods of computation in the rotated frame of reference see Section 3(a)(3) in Hewson (2009a). Note also that masking inequality WM5, the ‘wave anti-wave discriminant’ for frontal waves, could be replaced with  $\zeta_{di} > 0$ . The two are equivalent. This implies that the disturbance vorticity concept helps define frontal waves as well as diminutive waves.

In summary, this section has described how graphical devices such as contouring and colour-filling, when combined with suitable locating and masking diagnostic variables, can be used to pinpoint cyclonic features of various types. Diagnostic variable sets pertaining to the three feature types in the conceptual model on Figure 1 have also been introduced.

### 3. Feature detection

#### 3.1) Requirements

Converting semi-mathematical definitions of cyclonic features into workable sets of diagnostics (as on Table I) is not trivial. This section thus aims to provide a full justification for each of the diagnostics used to identify diminutive waves and barotropic lows. Frontal wave diagnostics have already been covered in Hewson (1997). Additionally, examples here illustrate how the higher level directional derivatives (required for some diagnostics) can be computed in such a way that feature identification is not disrupted with noise.

#### 3.2) Diminutive waves

##### 3.2.1) Diagnostic selection

The first part of the diminutive frontal wave definition (in Hewson, 2009a) states that:

*“the tip of a diminutive wave exists wherever, on a low level front, the vorticity of the cross-front geostrophic wind reaches, in the along-front direction, a local maximum...”*

The second part states that:

*“...provided there is neither a frontal wave nor barotropic low in the vicinity”*

Diminutive waves are illustrated on Figure 1 (stage 1), and are mathematically defined by the top section of Table I, with different rows representing different aspects of the first part of the above definition. At the outset this definition requires coincidence with a front. The front is represented, after Hewson (1998a), by locating equation DL1, which picks out the warm air sides of baroclinic zones, and masking inequalities DM1 and DM2, which relate to local thermal gradients. Maxima in the vorticity of the cross-front geostrophic wind, i.e. the ‘disturbance vorticity’ (see Equations (1) and (2)), are then simply identified via locating equation DL2, and masking inequality DM5. DL2 shows where the gradient of the disturbance vorticity, computed in the along-front direction, is zero, thereby representing an along-front turning point in the value of that vorticity. Masking inequality DM5, which is diagnostic DL2 itself differentiated in the along-front direction, retains only those turning points that are maxima. Mask DM6 represents an additional constraint, namely that the disturbance vorticity must be positive. Including this ensures that nominal frontal rotation, in so far as it relates to the geostrophic wind, is cyclonic. Some tuning was applied which elevated the threshold for DM6 above zero. This was to try to ensure that one could visually identify, in the isobaric pattern, at least some change in along-front spacing, which would have been the first clue, to the synoptician, of the appearance of a diminutive wave (reference the slight opening out of the isobars at stage 1 on Figure 1). Finally, it was found helpful, also for pragmatic reasons, to introduce masks DM3 and DM4. Mask DM3 impacts on the frontal aspect of the definition, helping eliminate some ‘warm-conveyor belt fronts’. These are usually associated with humidity rather than thermal gradients, and were identified in Hewson (1998a) as being one disadvantage of using wet bulb potential temperature (or equivalent potential temperature) rather than potential temperature as the locating thermal variable. Mask DM4, which retains features only where the full relative vorticity is greater than zero, was added as a final mask in order to improve representation of cyclonic features in some coastal regions and regions of higher orography. Though introduction of this was fundamentally pragmatic, it is not at all unreasonable to require that any cyclonic feature have a full vorticity signature that is itself cyclonic.

### 3.2.2) Example

The viability of using along-front derivatives of the cross-front wind (DM6, DL2 and DM5 on Table I) to automate the detection of diminutive waves will be demonstrated with an example. Figure 4 shows a snapshot, south of Greenland, from a model forecast in which a cold front was objectively identified; note the dashed black line and associated troughing in the white height contours. The same case was displayed on Figure 4 in Hewson (2009a). The geostrophic disturbance vorticity, shown in colour on Figure 4a, was computed as described in Hewson (2009a), and represents diagnostic DM6. Arrows denote points at which along-front maxima ( $A_n$ ) and minima ( $B_n$ ) of this field were determined visually, clearcut turning points being denoted by solid arrows and more marginal cases by broken arrows. Locating diagnostic DL2 is the along-front derivative of the disturbance vorticity; its zero contours are also plotted on Figure 4a (black solid, both sides). Evidently each of the ‘clearcut’ maxima and minima (B1, A1, B2 and A3) corresponds with an intersection point (blackened) of the black contours of DL1 (the front) and DL2, to within about half a grid-spacing. Out of the four ‘marginal’ maxima and minima (A2, B3, B4 and A4) two (A2 and B3) correspond with an intersection point. For the other two (B4 and A4), intersection points were almost present; note the small zero contour ‘pip’ just SE of the B4 arrow. This all suggests that diagnostic DL2, represented by simple finite differencing, can successfully pick up the main turning points in an along-front profile of the disturbance vorticity, which is a primary requirement for automated identification of diminutive waves. Figure 3f would identify these six points graphically. Meanwhile diagnostic DM5 (the along-front derivative of DL2) shown in colour on Figure 4b, needs to successfully identify the nature of each of the turning points; the dividing line between maxima and minima, i.e. zero, lies along the green-yellow boundary. Each contour intersection that is a maximum (A1, A2 and A3) lies where DM5 is positive, whilst all the minima (B1, B2 and B3) lie where DM5 is negative (though the less well-defined B3 is very close to the boundary; probably a model resolution limitation). Therefore when mask DM5 is graphically applied (Figures 3g and 3h) the three minima (B1, B2 and B3) would be successfully erased. Finally note how in this particular instance ‘marginal’ maximum A4 lay in a region where the geostrophic disturbance vorticity, at about  $1 \times 10^{-6} \text{ s}^{-1}$ , was much less than the Table I threshold for DM6 of  $8 \times 10^{-6} \text{ s}^{-1}$ . Conversely, the other maxima (A1, A2 and A3) lie where this vorticity is  $10\text{--}15 \times 10^{-6} \text{ s}^{-1}$ , which is above the threshold, and so these points would have been retained when additional mask DM6 was applied (again corresponding to Figures 3g and 3h). This all demonstrates that the automated method provides the required result: when the relevant diagnostics are calculated, and post-processed graphically as on Figure 3, the tips of diminutive frontal waves are successfully detected.

### 3.3) Barotropic lows

#### 3.3.1) Diagnostic selection

First note that the reason our low pressure centres are referred to as ‘barotropic lows’ relates to the hybrid identification methodology employed, and to post-processing of the related output; this is discussed in Section 4.

To identify a low pressure centre (which after post-processing becomes a ‘barotropic low’), the approach taken here is simply to pinpoint minima in a low level (1000 hPa) geopotential height field, though using a mean sea level pressure field instead would be equally valid. On a horizontal grid all 2-dimensional minima coincide with the intersections of zero contours of two orthogonal first derivatives of the pressure or height field (BL1 and BL2 on Table I). Although these derivatives are clearly not invariant under local co-ordinate rotation, the intersection points are. The set of intersection points also includes unwanted maxima and saddle points (i.e. cols) which are

both removed via masking (Figures 3g and 3h). Maxima are simply removed by ensuring del-squared of the input field is positive (BM1 on Table I). Some pragmatic tuning is incorporated at this stage, by elevating the threshold above zero, and by filtering BM1 as described. This tuning was necessary for two reasons. Firstly it prevents the proliferation of centres that show no temporal continuity, at least on 12-hour timescales, in slack pressure gradient regions (complex lows in particular). Secondly it reduces the appearance of stationary lows over high model orography (single gridpoint peaks in particular) where the method used for hypothetical underground height extrapolation is always contentious (see Chen and Bromwich, 1999). Here sub-surface heights were computed using model low-level thicknesses, and the assumption of a standard lapse rate within this layer and underground. Mask BM1 will in practice also remove those saddle points classified synoptically as anticyclonic cols. Removal of cyclonic cols is more complex, and requires the introduction of mask BM2, which is the product of orthogonal second derivatives of the height field. These must be computed using carefully selected local co-ordinates that run parallel and perpendicular to average height contour orientation in the vicinity. In practice these co-ordinates run along and across the col's major axis; they are computed using the 5-point mean axis methodology (Hewson, 1998a) applied to height field gradient vectors.

### 3.3.2) Example

Figure 5 provides an example of the four low centre diagnostics computed from gridded model data (contoured in blue (BL1 and BL2), contoured in pink (BM1) and shaded in colour (BM2)) together with the input 1000hPa geopotential height field (thick white) from which they were all calculated. All blue contour intersection points are labelled. The intersection at X1 clearly denotes a low centre, where diagnostics BM1 and BM2 are both well above threshold, implying that this point would be retained through to Figure 3h. The X2 intersection is an anticyclone centre, where del-squared of the height field (BM1) is negative, and therefore below its threshold of  $+1.0 \times 10^{-9} \text{ m}^{-1}$  (contoured), implying removal during masking. Point X4 is not a low centre but lies in a cyclonic col region, where BM1 is just above its threshold. This point would however be successfully removed by mask BM2 which is negative here, and thus below its threshold (0). Finally, point X3 is a borderline case that clearly satisfies the BM1 inequality, but only just satisfies BM2. Close scrutiny of geopotential height data (not shown) indicates the weakest of pressure minima at this point. Thus graphical application of the Table I criteria for barotropic lows successfully pinpoints and isolates just two low centres on Figure 5, at X1 and X3.

### 3.4) Discussion

Figure 5 and the accompanying description provide one complete real-world example of the 'intersecting contours method' being used for feature detection, the features in question here being low pressure centres. It should be highlighted that the equation set comprising BL1, BL2, BM1 and BM2 is in fact generic, meaning that it will find minima (or maxima) in *any* 2-dimensional scalar field if  $\phi_{1000}$  is replaced with that scalar (and with the BM1 threshold and any filtering adjusted according to purpose). Moreover, if one had wanted to focus (in a different study) on col points, to look at deformation for example, those too could be easily isolated, merely by altering the threshold for BM1, and the sign of the BM2 inequality.

The intersecting contours method has three particularly attractive characteristics:

1. Simplicity; the diagnostics can be computed relatively easily.
2. Visibility; intrinsic to the graphical processing stage is the immediate visualisation of algorithm performance (Figures 4 and 5).

3. Precision; interpolation inherent in contouring enables extrema to be pinpointed at a spatial resolution higher than that of the grid, which in turn facilitates identification of smoother cyclone tracks.

For identifying extrema in 2-D meteorological fields it is the ‘calculus-based’ method of Benestad and Chen (2006) that most closely resembles ours. Benestad and Chen use a cylindrical lat-long grid, and equations equivalent to BL1, BL2 and BM1 to identify the extrema, though they employ no mechanism to deal with cyclonic cols that have a diagonal orientation (BM2 here). Additionally, instead of using surface fitting implicit in the contouring, they use polynomial fits in orthogonal directions derived from least squares regression.

Other published methods for finding 2-D minima or maxima used in meteorology, range from very simple gridpoint searching (e.g. Serreze *et al* (1997), Hanson *et al* (2004)), to the complex feature-based centre-of-mass algorithms found in Hodges (1994), to the surface-fitting techniques of Murray and Simmonds (1991), Hodges (1995) and Pinto *et al* (2005). The surface-fitting techniques could give feature positions that differ slightly from those provided by BL1 and BL2, though whether these positions would be better is questionable, and indeed any differences would only have practical relevance if the input data were upscaled prior to algorithm application, which is not the case here.

To recap, this section has discussed and illustrated which new diagnostic sets are needed to enable two types of cyclonic feature to be pinpointed in numerical model output, when using the intersecting contours method described in Section 2.3. The feature points in question are the tips of diminutive frontal waves, and the centres of (barotropic) lows, and together with the frontal wave diagnostics described in Hewson (1997) form a complete method for detecting virtually all cyclonic features in the lower troposphere.

## 4. Post-processing

The post-processing steps are a new and essential part of the identification methodology we employ, and will be described here.

To ease comprehension here, we will first assume that out of the five classes of cyclone that are actually identified we only need to deal with the three that are most prominent, namely standard frontal waves, standard diminutive waves and barotropic lows. Reference to the fourth and fifth classes, namely thermally weak frontal waves and thermally weak diminutive waves, which are denoted by the smaller spots on Figure 2a, is left to the end of this section.

Once provisional feature points have been detected, at a given time, using the methodology of Sections 2 and 3, post-processing needs to address two problems. These problems are labelled ‘borderline cases’ and ‘definition overlap’, and are necessarily addressed by the post-processing in that order.

### 4.1) *Borderline cases*

A ‘borderline case’ is where a cyclonic feature point is poorly defined. The distinctiveness of such a point depends primarily on the angle between tangents to the locating contours at their point of intersection (conformal map projection assumed). Perpendicular tangents imply a high confidence,

well-defined centre (e.g. centre X1 on Figure 5<sup>†</sup>) whilst a small angle implies a lower confidence less well-defined centre (e.g. centre X3 on Figure 5). For angles approaching zero a string of several closely-spaced intersection points can occasionally occur. These need to be reduced to a single centre of gravity point. This is done, for each cyclone type separately, by forming a separation matrix for *all* intersection pixels identified across the full domain by the graphical processing (Figure 3h). Provided the closest two points are closer together than a pre-defined threshold minimum separation they are combined into a single halfway point, after which the separation matrix is recomputed with one row and one column removed. This clustering procedure is repeated until the minimum separation anywhere in the matrix exceeds the threshold. The process is illustrated on Figure 6; note how the clusters of three green pixels and two orange pixels on Figure 6a are each reduced to single pixels on Figure 6b.

In practice the above clustering will also combine, on occasion, pairs of closely-spaced intersection points that themselves are each defined by contours that are nearly orthogonal. Such a scenario can occur if there is a minor, localized intersection point of the opposite sense inbetween; Figure 4 provides an example; note how A2 and A3 (denoting along-front maxima in disturbance vorticity) are close together and are separated by minor minimum B3.

The separation threshold we currently use is 300 km. This is mainly pragmatic. However there is also some mathematical consistency, because to satisfactorily represent a wavelike structure in a field (a sine wave in its simplest form) requires at least 4 gridlengths, and the points on the re-projected grids that we use are typically about 50 km apart.

#### 4.2) Addressing overlapping definitions with a cyclone hierarchy

The ‘definition overlap’ problem arises out of using a hybrid technique (rather than other authors’ univariate techniques) and requires particular attention. If unchecked it would lead to centre proliferation, and ambiguities in cyclone type due to double or treble counting; for example a frontal wave tip might also be a low pressure centre. To overcome this, a cyclone-type hierarchy is applied, using a ‘co-location mask’ to remove all adjacent occurrences of types lower down the hierarchical list. This requires one input threshold, namely the minimum cyclone separation, which will be the same as that used above for borderline cases. As discussed in Hewson (2009a) the hierarchical list is, in order of preference:

- Standard frontal wave
- Barotropic low
- Standard diminutive wave

The procedure begins at the bottom of the list, by removing every diminutive wave that is closer to a barotropic low than the minimum separation threshold. Then, moving up the hierarchy, frontal waves are introduced, with any barotropic lows or remaining diminutive waves that are closer to one of these than the threshold also being removed. Figures 6b and 6c provide a hypothetical example; note how three separate ‘clusters’ are reduced to single points according to the hierarchy.

Recall from Section 3.2.1 that the second part of the diminutive wave definition indicated that there should be ‘neither a frontal wave nor a barotropic low in the vicinity’. This aspect has now been incorporated, with proximity defined by the separation threshold (which is the same for both post-processing stages - 300 km).

<sup>†</sup> Figure 5 is not strictly on a conformal projection but for the purposes of qualitative illustration is sufficiently close.

1  
2 Referring back to the cyclone model in Figure 1, recall that ‘frontal waves’ account for the majority  
3 of the life cycle shown. This is because they take priority in the cyclone type hierarchy. Diminutive  
4 waves simply apply to stage 1, whilst barotropic lows apply to stages 6 and 7.  
5

6  
7 Furthermore, note that any identified low pressure centres (Figure 6a) that survive post-processing  
8 (Figure 6c), will implicitly *not* have a front associated with them, because those that do will have  
9 been retained instead, through the hierarchy, as frontal waves. It is for precisely this reason that we  
10 use the term ‘barotropic’ to describe such a low. Whilst the order selected for the hierarchy is  
11 somewhat subjective, the one chosen has the clear advantage of disentangling frontal features from  
12 non-frontal. In turn this relates closely to the energetics of extra-tropical cyclones and the  
13 conversion of available potential energy (in a baroclinic (frontal) environment) into kinetic energy  
14 (in a barotropic environment) during growth. If frontal waves were put beneath low centres in the  
15 hierarchy this dynamical connection would be lost.  
16  
17

18  
19 From a standpoint of pure juxtaposition one could suggest that a low pressure centre coinciding  
20 with a *spread-out* thermal gradient is a somewhat baroclinic low that would, by our scheme, be  
21 classified as barotropic. However, this hypothetical scenario ignores the dynamics-driven proclivity  
22 for a broad thermal gradient region to readily collapse, through positive feedbacks, into a more  
23 focussed band or bands of large gradient at low levels, particularly when a low centre is forming.  
24 One mechanism for this collapse is thermal advection by non-uniform ageostrophic winds (as in  
25 semi-geostrophic theory, see Hoskins, 1982). Experience also suggests that the aforementioned  
26 hypothetical scenario rarely occurs in the real world.  
27  
28

29 Finally recall that we have not yet discussed how thermally weak frontal waves and thermally weak  
30 diminutive waves are dealt with. One could choose to omit these, but because they sometimes  
31 evolve into major cyclones, they are in fact retained. So the true processing actually involves five  
32 features, not three, from the outset, with ‘weak frontal waves’ and ‘weak diminutive waves’  
33 situated at the end of the quoted hierarchy, in that order.  
34  
35

36 To recap, sections 4.1 and 4.2 have discussed how meaningful but unwanted artefacts of the  
37 graphical processing methodology are successfully dealt with, and also how the ‘definition overlap  
38 problem’ can be overcome by application of a cyclone type hierarchy.  
39  
40

## 41 42 **5. Synoptic validity**

43  
44 To ascertain how successful the methods we have discussed are at identifying cyclonic features, a  
45 simple comparison was performed alongside the synoptic (front and mean sea level pressure) charts  
46 routinely produced by the Met Office duty chief forecaster. This is quite a stringent test but is seen  
47 as a necessary step, particularly as one aim at the outset was to ‘replicate synoptic practice’. Most  
48 previous climatological studies of cyclonic activity, whilst they may show one example, have not  
49 generally performed detailed comparisons over an extended period. A noteworthy exception to this  
50 is the study of Pinto *et al* (2005), which is further discussed in Sections 6.2 and 6.4.  
51  
52

53  
54 A small area west-southwest of the UK was selected for the comparison, bounded by latitudes 50°N  
55 and 55°N, and longitudes 10°W and 20°W. For weather prediction for the UK, given the prevailing  
56 west-southwesterly flow, this key region merits a high degree of attention from the forecaster  
57 preparing surface analyses. The cyclonic centres and frontal waves that they identify in this area  
58 will thus generally have sound justification, from surface observations and/or satellite imagery.  
59 They should also be of a scale not dissimilar to that found in model data (60 km gridlength at that  
60 time). Over the UK, by comparison, forecasters tend to represent rather more mesoscale features on

1  
2 their analyses. This is because there is more data to identify them by; surface observation density is  
3 much higher, and 5 km radar data are routinely available.  
4

5  
6 The analysis period comprised winter months (November to April) between January 2000 and  
7 January 2005. Features on one synoptic analysis per day (0000 UTC) were compared with features  
8 identified objectively from corresponding model analysis fields. Examples of the types of synoptic  
9 and objective charts used can be seen on Figure 9. In order to register a cyclonic feature, the  
10 synoptic chart had to show a low pressure centre (denoted by a cross) or a frontal wave tip, whereas  
11 the objective chart had to show an objective barotropic low centre or an objective frontal wave tip,  
12 with standard Table I thresholding applied (diminutive waves could not be verified directly as it has  
13 not been synoptic practice to plot them). By these measures the 'true' (synoptic chart) cyclonic  
14 feature frequency, within the box, was 4.6 per month. On the objective charts, it was about 3.2 per  
15 month (i.e. 68%). When a feature was registered on both objective and synoptic charts, it was  
16 counted as 'correct identification'. By this strict, unadjusted measure 2.3 of the 4.6 synoptic  
17 cyclonic features per month (i.e. 50%) were correctly identified. Equivalently, 2.3 synoptic features  
18 per month had no objective counterpart ('misses'), whilst 0.9 objective features per month had no  
19 synoptic counterpart ('false alarms'). Table II lays out the reasons for the misses and false alarms,  
20 as ascertained by visually comparing charts in and around the verification box.  
21  
22  
23

24  
25 Row 1 cases represent small positional differences near the box boundaries (mean separation =  
26 70 km); these are caused partly by model resolution, and partly by there sometimes being a slight  
27 separation of frontal wave tip (on the objective chart) and low pressure centre (on the synoptic  
28 chart) late in a cyclone life-cycle (e.g. frame 5 on Figure 1). As ill-defined (barotropic) low centres  
29 were deliberately excluded from the objective identification by masking (see Section 3.3.1) it is  
30 unsurprising that such features are the largest contributor to the 'misses' (row 2 ). Moreover, half of  
31 these were considered of dubious validity when compared to the pressure pattern on the same  
32 synoptic chart, perhaps reflecting alternative use of a 'cross' by the analyst to signify a 2-  
33 dimensional cyclonic inflection point in the pressure field that is not strictly a low centre (an 'open  
34 depression' in the terminology of Murray and Simmonds (1991) and Pinto *et al* (2005)). Rows 3  
35 and 4 can be considered together in that they probably also signify pragmatic use of available  
36 symbols, by the analyst, in circumstances where alternative but as yet unfamiliar symbolic notation,  
37 for a diminutive wave for example, might have been more correct. Row 5 highlights resolution  
38 limitations, whilst row 6 is an assimilation issue, which would invite discrepancies with any  
39 identification scheme. Rows 1 to 6 on Table II thus represent areas where objective-synoptic chart  
40 discrepancies are not considered serious; indeed many are inevitable.  
41  
42  
43

44  
45 The remaining two rows signify potentially more serious weaknesses in the objective techniques.  
46 Row 7 illustrates that there are occasions when meteorologically significant linear features,  
47 possessing low-level wet-bulb potential temperature / potential temperature gradients that are very  
48 small, are plotted as fronts, and that cyclonic features sometimes form on these fronts. Here the  
49 forecaster, in preparing their analysis, is able to distort the usual subjectively-applied rules for  
50 pragmatic, weather-related reasons. A fully objective technique could not do this without  
51 introducing 'either/or' logic into definitions that would greatly complicate the interpretation of  
52 results. Row 8 is the largest contributor to the so-called 'false alarms'; this relates to near-stationary  
53 or stationary fronts. Again the forecaster can seemingly gain an advantage here by identifying when  
54 and where a frontal wave is forming (partly using imagery) and by then using warm and cold front  
55 symbols, and suitable frontal curvature, to signify a wave. Sometimes the objective technique can  
56 'stutter' as a result of the angle between objective front and thermal advection contours (WL1 and  
57 WL2 on Table I) being very small. This is referred to in Section 4 as a 'borderline case'. However,  
58 there were occasions, during the comparison, when an objective wave, in such a situation, did  
59  
60

1  
2 evolve into a much more substantial feature that was not highlighted until later on the synoptic  
3 charts. Thus it can often be a moot point as to what constitutes truth in these marginal situations.  
4

5  
6 If one discounts the somewhat inevitable discrepancies contained in rows 1 to 6 on Table II, then  
7 for the objective techniques the hit rate becomes 84%, and the false alarm ratio 17%. Thus the main  
8 conclusion from this comparative study is that the replication of cyclonic synoptic features by the  
9 recommended objective techniques, whilst not perfect, is generally good. Reference should also be  
10 made to Mass (1991), where different forecasters provided with the same data analysed fronts  
11 differently; the implication then is that *perfect* replication of subjectively-drawn synoptic features is  
12 in any case impossible.  
13

14  
15 To facilitate comparison with other published studies it will be assumed, not unreasonably, that the  
16 5-year period considered provides a moderately representative estimate of a longer period cyclone  
17 climatology. The 'true' and 'objective' cyclonic feature frequencies of 4.6 and 3.2 days per month  
18 respectively, quoted above (for 50-55N, 10-20W), can then be compared with suitably normalized  
19 values from other studies for the same region. In Hoskins and Hodges (2002), who use 450km  
20 resolution data over 22 years, the corresponding 850mb vorticity maximum feature frequency is  
21 about 1.6 days per month (35% of 'true'), whilst the mean sea level pressure minimum frequency is  
22 about 0.6 days per month (13%). In Sickmüller *et al* (2000), who use 120km data over 18 years, the  
23 corresponding 1000hPa height minimum feature frequency is about 0.6 days per month (13%).  
24 These amount to even larger shortfalls compared to the synoptic charts. Whilst analysis period  
25 inconsistencies will have had an impact, the primary causes of the shortfalls are likely to be lower  
26 spatial resolution of input data (see Blender and Schubert, 2000), simpler identification  
27 methodologies, and different thresholding methods. In particular this comparison re-iterates the  
28 limitations of using surface pressure minima (or equivalently 1000hPa heights) in isolation, even at  
29 higher resolution, as Hoskins and Hodges and others have recognised. However note at the same  
30 time that when using intrinsically the same parameter but vastly different resolutions the two cited  
31 papers arrived at the same frequency. This all serves to re-emphasise that tracking of cyclonic  
32 features is far from being a clear-cut procedure. Finally note also that the detrimental impact of  
33 extraneous factors such as map projection (Hodges (1995, 1996) and Zolina and Gulev (2002)) on  
34 feature frequency is of order 10%, and as such looks to be about an order of magnitude less than the  
35 impact of not using a multifaceted identification method.  
36  
37  
38  
39  
40

41 To summarise, this section has performed a detailed comparison, for a small oceanic region,  
42 between cyclonic features marked subjectively, on synoptic charts, in real time, by forecasters and  
43 those identified objectively in model analyses. The agreement level for our objective methodology  
44 was on the whole found to be very good. Conversely, in two other studies using different  
45 identification methods the objective feature frequency in this region was relatively low.  
46  
47  
48  
49

## 50 6. Tracking

51  
52 The natural next step in the lifecycle identification process is to connect the features across time.  
53 Existing schemes, notably Terry and Atlas (1996) and Simmonds and Murray (1999), were  
54 evaluated for suitability. These had been developed primarily to track widely-spaced, large  
55 cyclones, initially pinpointed using mean sea level pressure minima *or* relative vorticity maxima.  
56 For the cyclonic features described in this paper, which are relatively common, which can be  
57 relatively close together and which are identified in a variety of ways, the existing schemes were  
58 not well-suited. Thus a new and specially tailored feature-tracking scheme was developed.  
59  
60

The primary aim of tracking is to link each root feature (R), at each output time, to a particular candidate feature (C) at the next output time, provided of course that a suitable one exists. By repeating this process for all times feature tracks of varying lengths and durations are put together.

### 6.1) Tracking methodology for each time step

At each time, for each R feature, the processing involves up to two checks. Before the checks every C feature is a possible match for every R feature. Together, the checks remove the vast majority of those possibilities. Once all checks have been completed for all R, an iterative process based on the results then finally links the Rs to the Cs for that time step.

So for each R the checks proceed as follows. In check 1 some (or all) C features are discarded, based on 'half-time separation' (defined below) which must be below a threshold distance. Then, if one or more C features remain, check 2 proceeds, in which a non-dimensional 'likelihood score' (L) is computed for each one. L is based on three independent 'likelihood parameters', so selected to imitate the manner in which a synoptician would associate features on charts. The parameters themselves each relate, therefore, to transition probability. The parameters are (i) 'half-time separation' (same as used in check 1), (ii) 'feature type transition' and (iii) 'thickness change'. Check 2 ends with any C feature whose likelihood score lies below another threshold being discarded.

The three likelihood parameters are described below, with reference to Figure 7. On Figure 7 the root feature is 'R' (at time  $T_0$ ), and the candidate features at the next time ( $T_1$ ), that have passed check 1, are  $C_1$ ,  $C_2$  and  $C_3$ .

- i) *Half-time separation ( $d_i$ ):* 'Half-time' ( $T_{\frac{1}{2}}$ ) is defined to be  $0.5 \cdot (T_1 - T_0)$  hours after  $T_0$ . From  $T_1$  each candidate (C) feature is back-tracked to a half-time position  $C(T_{\frac{1}{2}})$  using  $(-1) \cdot 60\%$  of the 500 hPa wind velocity directly above it at  $T_1$ , appealing to the notion of an upper level 'steering wind' for cyclones, as in Terry and Atlas (1996). Meanwhile for the root (R) feature, previous history determines which of two different forward-tracking methods are employed to estimate its half-time position,  $R(T_{\frac{1}{2}})$ . If there is no previous history, then  $(+1) \cdot 60\%$  of the 500 hPa wind is used to advance the feature. However if there is previous history, two estimation methods are given equal weight: steering wind, as above, is one; extrapolation, preserving system velocity in the previous time step, is the other. Half-time separation  $d_i$  for a candidate  $C_i$  is then simply the distance  $R(T_{\frac{1}{2}}) \rightarrow C_i(T_{\frac{1}{2}})$  in km. On Figure 7 estimated half-time positions are those in the central grey polygon, whilst half-time separations for candidates  $C_1$ ,  $C_2$  and  $C_3$  are  $d_1$ ,  $d_2$  and  $d_3$  respectively. These are also represented on the inset (dotted lines).
- ii) *Feature type transition :* To denote type transition probability for each candidate a look-up table score (S) is allocated. Scores are based on percentage frequencies of transitions in a manually-analysed dataset, given in Table 2 in Hewson (2009a). Tabulated values are subtracted from 100 so that smaller means more likely. As an illustration consider Figure 7, and for convenience assume that R,  $C_2$  and  $C_3$  are standard frontal waves, and that  $C_1$  is a standard cold front diminutive wave. The aforementioned table indicates that after 12 hours, on average, 5% of standard frontal waves evolve to become a standard cold front diminutive wave, whilst 63% remain as standard frontal waves. So these particular 'transitions' are allocated, respectively, scores of 95 ( $C_1$ ) and 37 ( $C_2$  and  $C_3$ ). Scaling in Equation (3) below then adjusts the transition type score for  $C_2$  and  $C_3$  to zero, consistent with 'frontal wave to frontal wave' being the most common transition of all. This is represented graphically on the Figure 7 inset.
- iii) *Thickness change:* 1000-500 hPa thickness at each C point (at  $T_1$ ) is subtracted from 1000-500 hPa thickness at the R point (at  $T_0$ ). Hypothetical values were used on the Figure 7 inset.

The Likelihood score ( $L_i$ ), for each candidate  $C_i$  is then a scaled combination of the separation, type and thickness scores (in km). The aim is to find the best pairing in 3-D space, for R, using a least-squares approach:

$$L_i = \sqrt{d_i^2 + (\alpha_t t_i + \beta_t)^2 + ((\alpha_z z_i + \beta_z)/2)^2} \quad (3)$$

Where  $L_i$  = Likelihood score for candidate feature  $C_i$   
 $d_i$  = 'Half-time separation' of R and  $C_i$  in km (i)  
 $t_i$  = 'Feature type transition' score (ii)  
 $z_i$  = 'Thickness change' (1000-500 hPa) between R and  $C_i$  in dm (iii)  
 $\alpha_t, \beta_t, \alpha_z, \beta_z$  = Constants

Initially the intention had been that the three components ( $d_i, t_i$  and  $z_i$ ) would have equal weighting. The range of values for each component was extracted from a number of cases, with constants then adjusted so that the mean and standard deviation of the contributions from both  $t_i$  and  $z_i$  matched those of  $d_i$ . This gave values of  $\alpha_t=8.59, \beta_t=-318, \alpha_z=39.0$  km/dm and  $\beta_z=208$  km/dm. Subsequent forecaster feedback regarding incorrect tracking lead to further tests, after which the thickness change component weight was reduced by half, as in Equation (3).

Pragmatic testing also resulted in the following thresholds being set for discarding candidates during the feature association procedure:  $d_i > 600$  km in check 1 and  $L_i > 700$  km in check 2.

After applying the two checks for all possible (R,C) combinations, the final, iterative part of the tracking (for a given time step) can proceed. In this all (R,C) pairings to have survived the checks are ranked in terms of their Likelihood scores, with the most likely (lowest) first. These are all worked through in order, with the first (R,C) pairing being automatically accepted as part of a feature track, and then subsequent (R,C) pairs also being accepted providing they do not relate to an R or a C that has already been associated. If no valid future position can be found for any root features R then their respective tracks are ended. Similarly, if no previous position can be found for any candidate features C then they will each form the starting points of new tracks. It should also be noted that some features will exist for one time only, and will therefore have no prescribed track. This is a consequence of the finite interval between time frames, and is an issue with all tracking algorithms.

## 6.2) Comparison with previous studies

Raible *et al* (2008) and others have highlighted how track discrepancies can arise from using different tracking methods. It is useful therefore to briefly contrast methodologies found in previous tracking studies with the approach used above. There are many differences, but one key one is that it has been commonplace for feature association to be effected not at  $T_{1/2}$ , but at  $T_1$ , which we will refer to as 'full-time tracking' (e.g. Sinclair (1994), Terry and Atlas (1996), Simmonds *et al* (1999), Pinto *et al* (2005), Wernli and Schwiertz (2006)). At the outset that approach was trialled, but again forecaster feedback highlighted some missed associations, which disappeared when half-time tracking was used instead. This enhancement has proved especially useful for some rapid cyclogenesis cases where steering winds and system velocity, associated with the developmental left-exit regions of upper level jets, can vary greatly. Examples of this behaviour can be seen on Figure 2b, highlighted in purple. Note how the frontal wave just north of Scotland (top panel) slows

1  
2 down markedly and turns to the left as it develops into a barotropic low. The feature entering  
3 Hudson Bay behaves similarly.  
4

5  
6 Note also that many previous studies do not estimate the position of R at T1 but just look for the  
7 closest spatial match, amongst all the T1 features, to R's position at T0 – the so-called 'nearest  
8 neighbour' approach (e.g. Blender and Schubert (2000), Sickmüller *et al* (2000), Geng and Sugi  
9 (2001), Hanson *et al* (2004)). This can work satisfactorily for a small number of large, well-spaced  
10 features, but would be an unequivocal failure if used here, due to the wide range and large number  
11 of features identified, some of which move very rapidly (e.g. frontal waves near strong jets), others  
12 which are almost stationary (e.g. some old barotropic lows). Again many examples can be found on  
13 Figure 2.  
14

15  
16 One study employing a sophisticated method for estimating R's future position is Ayrault and Joly  
17 (2000); interestingly they use steering winds at two levels. The iterative method of Hodges (1996),  
18 looking both forwards and backwards in time to smooth out system trajectories, possesses some  
19 synoptic realism, although one aim there is to minimize system acceleration/deceleration, which  
20 might be problematic when trying to track the aforementioned left-exit features.  
21  
22

23  
24 Pinto *et al's* (2005) approach has some connection with the present study, in that they give weight  
25 to both previous motion and a steering wind to estimate future position, and then use full-time  
26 tracking based on that. However for space-saving reasons the steering wind is not upper level but is  
27 based on the average surface geostrophic wind in a ring around the feature.  
28

### 29 *6.3 Half-time tracking and time intervals*

30

31  
32 The Appendix shows how using half-time tracking with a time interval  $\Delta T$  can, in idealized cases,  
33 give more reliable feature association than would full-time tracking with a time interval of  $0.5(\Delta T)$ .  
34 Importantly, this result means that with half-time tracking introduced the time interval between  
35 frames can in principle be doubled without a loss of tracking integrity. In turn this means a halving  
36 of computation time, because computation time depends primarily on the number of frames. The  
37 data storage requirement would also be halved. These two benefits can be realised in research when  
38 post-processing climate runs and climate ensembles, and in operations when post-processing  
39 shorter-range ensembles for forecasters. Though not so critical in the former case, in the latter case  
40 the timeliness aspect is extremely important. Previously, Blender and Schubert (2000), have  
41 highlighted the big advantages of using a small time interval, such as 4 hours; it is however  
42 noteworthy that they used only the nearest neighbour approach, which, as they recognize,  
43 influences their conclusions. 'Half-time tracking', with 'steering wind' estimates, now looks to be a  
44 viable alternative, and has indeed helped us to successfully use a 12h time interval.  
45  
46  
47

48  
49 To apply a simple test of the tracking algorithm accuracy, eight consecutive time frames from an  
50 operational ECMWF (European Centre for Medium range Weather Forecasts) control forecast,  
51 covering an extended North Pacific domain, were selected for analysis (data time 0000 UTC 20<sup>th</sup>  
52 October 2008, frame time interval 12 h): this gave 163 possible transitions. A detailed subjective  
53 analysis determined the appropriate feature associations between consecutive time frames; these  
54 were compared with associations made by the automated tracking scheme. On only 3 occasions  
55 were the tracking scheme associations clearly wrong. Two of these instances involved weak coastal  
56 features in the vicinity of NW Mexico, which should have remained by the coast but were tracked  
57 inland. The third error occurred for a more substantial feature that should have exited the domain,  
58 north across Alaska, but which the tracking kept within the domain (partly because outside there  
59 are no recorded features with which to associate). Overall this suggests a tracking accuracy of order  
60 98%. This can be compared with 88% quoted in Gray and Dacre (2006) for when the Hodges

1  
2 tracker was applied to features described in the paper. Recall also that in that paper the weaker  
3 features were omitted, which markedly *reduces* the scope for incorrect associations. Here the  
4 weaker features were left in.  
5

6  
7 It should be re-iterated that testing was not limited to the one Pacific case, but was in fact a  
8 continual process, wherein forecaster feedback on tracking products provided for the North Atlantic  
9 domain, in real time, over a 2-3 year period, lead to concurrent modification and development of  
10 the tracker and its thresholds.  
11

12  
13 Whilst it is well established that low pressure centres and frontal waves can last for several days,  
14 one could ask whether the less developmental diminutive waves last long enough to be tracked at  
15 12 h intervals? If they were commonly very short-lived features, false associations could result.  
16 Using a 3 h interval Hewson (2009a) shows with examples that such features have coherent tracks  
17 that can last for 24 h and longer, so this is not a major concern.  
18

#### 19 20 6.4) Tracking of cyclonic windstorms 21

22 One clear motive for designing the techniques described in this paper was the desire to correctly  
23 capture and track all types of cyclonic windstorm (for examples see Figure 1 in Watkin and  
24 Hewson (2006), Figure 9 in Hewson (2009a), page 1273 of the September 2008 issue of *Bull.*  
25 *Amer. Meteorol. Soc.*, Figs. 9, 10 and 11 below and Figs 4-8 in Hewson (2009b)). In this regard it is  
26 helpful to provide some commentary on the specific challenges posed by cyclonic windstorms and  
27 how these were addressed, referring specifically to European examples:  
28  
29

- 30  
31 • For dynamical reasons cyclonic windstorms are commonly associated with very strong  
32 upper level jets (e.g. Lothar that hit France on 26 December 1999; see Wernli *et al*, 2002).  
33 As a result they can move very rapidly, and can also accelerate and decelerate rapidly (in  
34 the jet entrance and jet exit regions). Use of the steering wind and ‘half-time tracking’  
35 prevents these system velocity fluctuations from confusing the tracking algorithm, thereby  
36 avoiding association problems between time frames. In addition no constraints are placed on  
37 maximum displacement between frames. Most other techniques do not use steering winds or  
38 half-time tracking, and therefore in order to cater for the majority of cyclones, which move  
39 more slowly, have to impose maximum displacement constraints. Without this there would  
40 be extensive mis-association problems; the penalty is that the more extreme cyclones may  
41 not be catered for.  
42
- 43 • Cyclonic windstorms which cross land tend to fill there due to frictional effects, and this, in  
44 parallel with their more rapid movement over marine areas means they often have short  
45 lifetimes, as little as one day. For this reason a short lifetime cut-off, often seen in other  
46 algorithms (typically 2 days), is not applied here in any form. Note that in Hewson (2009a)  
47 29% of cyclonic features lasted less than 1 day, and 53% less than 2 days (from his Figure  
48 6), implying that this cut-off can have a very large impact.  
49
- 50 • Windstorm-generating cyclones can vary greatly in size, ranging from, say, the large Burns’  
51 Day storm that hit the U.K. on 25 January 1990 (McCallum, 1990), to the small but very  
52 intense windstorm (‘Renate’) that gave 100 mph gusts south-west of Bordeaux on 3 October  
53 2006. Devising techniques that can be applied at high resolution ensures that small storms  
54 will be identified as well as the large ones.  
55
- 56 • Polar lows can themselves lead to severe windstorms (e.g. low D in Hewson *et al*, 2000).  
57 These are intrinsically very small scale. Provided the model in use represents the feature,  
58 the algorithms will pick it up (as exemplified in Bracegirdle and Gray, 2007).  
59
- 60 • As they cross the ocean, the cyclonic features that lead to European windstorms can  
temporarily undergo a form of lateral compression in the central north Atlantic, between a

1  
2 large decaying mature cyclone in the Iceland-Scotland region, and an Azores high. This  
3 process has also been described as ‘along-front stretching by the environmental flow’, and  
4 is discussed in Renfrew *et al* (1997). Whilst in the compressed state the cyclonic feature  
5 commonly has no low pressure centre (see for example stage 2 on the lower panels in  
6 Figure 1), though one may have existed, to the west, earlier in its life cycle. Algorithms that  
7 rely on the existence of a pressure minimum will at best only represent this as two tracks,  
8 one in the west, one in the east, with a gap in-between, or at worst will discard both these  
9 via a minimum life-cycle cut off. Incorporating the frontal wave stage here enables the full  
10 tracks of such features to be identified. One real-world example was the North Sea storm of  
11 30 October 2000 (briefly described in Hewson, 2001) which, after being laterally  
12 compressed in the central North Atlantic, then evolved from a frontal wave with no closed  
13 isobars, to a large 950 hPa low with extreme winds, in just 9 hours as it crossed the UK.

- 14 • Cyclonic features that later lead to windstorms often develop on fronts characterized by  
15 strong thermal gradients and substantial low level (frontal) vorticity. Seeking out the  
16 maximum in the vorticity field, as many algorithms do, can be problematic in this frontal  
17 environment, due to the strip-like structure. The application of a vorticity partition, as is  
18 done here, gives a cellular structure (in the disturbance vorticity; see coloured field on  
19 Figure 4a) which relates specifically to diminutive waves. Maxima in such patterns are  
20 much easier to identify and track.

21 Discussion of the above issues is absent from many studies. A notable exception is Pinto *et al*  
22 (2005) who carried out extensive testing on documented windstorms, and then adapted their  
23 algorithms accordingly. In short the primary differences here, compared to that study, are that we  
24 use objective fronts, half-time tracking and high resolution data.

### 25 6.5) Summary

26 This section has described a new algorithm developed to track the cyclonic features described  
27 earlier in the paper. In the feature matching procedure the algorithm uses a 500hPa steering wind,  
28 ‘half-time tracking’ and multi-parameter comparisons. The half-time tracking aspect is completely  
29 new and looks to possess significant benefits compared to ‘full-time tracking’ used in many  
30 previous studies. Given the high feature density and large (12 h) time interval currently in use the  
31 association success rate is reassuringly high. Particular attention has been paid to successful  
32 tracking of all types of cyclonic windstorm.

33 Even when a tracking method appears successful, there will always be scope for further  
34 improvement. Here we could for example improve system velocity estimates using ‘steering’ winds  
35 at more than one level, and perhaps vary those levels according to feature type (see Ayrault and  
36 Joly, 2000). The weights for different feature type transitions could also be improved, to better  
37 account for the true transition climatology. The time interval between frames could also be reduced  
38 where practicable.

## 39 7. Applications

40 The real strengths of objective identification become apparent when manual post-processing  
41 becomes too costly in terms of resource and time; for example in climate runs, or when output from  
42 multi-member ensemble prediction systems (EPS) has to be analysed. Indeed application in the  
43 latter case has now advanced the feature identification concept into providing useful applications  
44 for operational forecasting. This aspect is illustrated and discussed in this section.

1  
2 The use of EPS in forecasting high-impact weather is particularly challenging. The standard,  
3 parameter-based methods for combining information from ensemble members, such as probability  
4 charts, suffer because point probabilities of severe weather are invariably low, and moreover  
5 because the lower resolution ensemble members can often fail to represent the intensity of the  
6 parameter in question. Current systems for forecasting high-impact weather such as the Met Office  
7 ‘first guess early warning system’ (Legg and Mylne, 2004) and the ECMWF ‘extreme forecast  
8 index’ (Lalaurette, 2003, and Zsótér, 2006), tackle this issue by recalibrating the data, but this can  
9 be unreliable for extreme events due to their rare nature. Although high-impact weather (severe  
10 gales, torrential rain etc.) often occurs on scales below those that the ensemble members can  
11 represent, those members can usually represent the causal features. The automated feature  
12 identification techniques described in this paper therefore have a key role to play in high-impact  
13 weather prediction using ensemble forecasts.  
14  
15  
16

17 The techniques to objectively identify fronts and cyclonic features have been applied to ensemble  
18 forecasts from the Met Office Global and Regional Ensemble Prediction System (MOGREPS),  
19 over a North Atlantic domain. In the MOGREPS system an Ensemble Transform Kalman Filter  
20 method is used to generate initial conditions that are added to the Met Office operational global  
21 analysis to create a 24-member ensemble (Bowler *et al*, 2008). The global medium-range version of  
22 MOGREPS runs twice a day, producing 12-hourly output for 15 days (T+0 to T+360) and is known  
23 as MOGREPS-15. It runs at a resolution of 1.25 degrees W-E by 0.83 degrees N-S (approximately  
24 90 km in the extra-tropics), with 38 levels.  
25  
26  
27

28 A ‘feature-based product suite’ has been developed specifically for use with ensemble forecasts, to  
29 display the objectively identified fronts and cyclonic features in both traditional and new and  
30 innovative ways. ‘Postage-stamp’ plots, a classic product used to display ensemble forecasts, are  
31 produced (not shown) showing the cyclonic features and fronts identified in each member at a set  
32 time, and in animation. Full-size animations of each member are also available for closer  
33 inspection.  
34  
35

36 Figure 8 shows a ‘spaghetti fronts’ chart, displaying fronts identified in all the MOGREPS  
37 ensemble members, for one case, for one lead time (36 h). Here we have not plotted the cyclonic  
38 features themselves, though existence of such is locally apparent from frontal configuration. There  
39 is evidently large spread, in the ensemble, to the west and southwest of the UK, in the handling of a  
40 cyclone and a following cold front wave. This would inform the forecaster to not rely too much on  
41 model handling of these particular features.  
42  
43  
44

45 Until now ‘spaghetti charts’ have commonly been used to show *continuous contours*, of, for  
46 example, specific values of 500 mb height or mean sea level pressure. There are two clear  
47 advantages of applying the concept to objective fronts. One is that there is a significant weather  
48 focus. The other is that regions of low gradient are automatically omitted through thresholding. On  
49 traditional spaghetti plots it is difficult to distinguish, visually, large spread in low gradient regions  
50 from large spread in high gradient regions; this is an important distinction because the latter case  
51 signifies much larger absolute variations within the ensemble.  
52  
53

54 Work is now underway to produce a cyclonic feature equivalent to the spaghetti chart animation,  
55 which will show coloured spots diverging with time instead of curved lines (for examples see  
56 Hewson, 2009b).  
57  
58  
59  
60

1  
2  
3 The addition of the tracking scheme as detailed in Section 6 has resulted in the ability to produce  
4 'storm track diagnostics' for the ensemble forecasts. Once features have been tracked across time in  
5 each ensemble member, a corresponding matching scheme takes each cyclonic feature in the  
6 ensemble control run, and cross-references or 'matches' it across the ensemble. The matched  
7 feature in each ensemble member is selected based on distance to the control run's feature position,  
8 on the feature type, and on difference in 1000-500 mb thickness, using a similar method to that  
9 used by the tracking scheme. The matching is currently only applied at T+0, as divergence in  
10 ensemble solutions makes reliable matching difficult at longer leads. For those longer leads a  
11 'strike probability' strategy is adopted instead, as discussed later.  
12  
13

14  
15 The storm track diagnostics will be illustrated using the case of an intense extra-tropical cyclone  
16 whose centre crossed northern Scotland on 31 December 2006 (see Figures 9c and 9d), and that  
17 gave gale-force winds over Northern Ireland, southern Scotland, and northern England. The storm  
18 was very high profile due to the related cancellation of several large New Year's Eve events. It also  
19 led to loss of power in thousands of homes, with structural damage to many properties. The storm  
20 was a rapidly developing feature, only appearing on analysis charts as a low pressure centre at 0000  
21 UTC 31 December 2006 (Figure 9c). Traditional cyclone identification and tracking methods that  
22 require a low pressure minima would have been very late in identifying this storm, but the new  
23 methods in this paper identify it 24 hours earlier, at 0000 UTC on 30<sup>th</sup>, as a frontal wave in the  
24 Atlantic (Figure 9b - compare with Figure 9a).  
25  
26

27  
28 Interactive web-based maps allow the user to click on any feature point in the control analysis plot  
29 (e.g. Figure 9b) to open up a new window which shows what track that feature then takes in all the  
30 ensemble members. Figure 10a shows tracks for the feature arrowed on Figure 9b. Though not  
31 shown here, the percentage of ensemble members that track a particular feature to each lead time is  
32 also indicated on the web page; if percentages are small the feature's development should be  
33 regarded as somewhat uncertain, even if the remaining members agree well. Alongside the tracks  
34 are displayed feature-specific plumes of various intensity measures, including mean sea level  
35 pressure and relative vorticity at the feature points, and maximum 1km wind strength and  
36 maximum 300 hPa jet strength nearby (see Figures 10b-f for these plumes for the aforementioned  
37 developing storm). The maximum wind strength at 1 km within a 600 km radius (Figure 10c), or  
38 300 km (Figures 10e), depending on system size, is a useful proxy for the maximum surface gust  
39 likely within the low's circulation, in relatively unstable air. By way of comparison note that  
40 Bengtsson *et al* (2009) used the maximum 925 hPa wind within a 5° radius in their storm track  
41 studies (which they usefully correlated with 10 m mean wind). This has the advantage of being a  
42 standard model output level, but has the disadvantage, compared to the 1 km level, of lying at  
43 different heights above, and locally below, the earth's surface. The maximum 300 mb jet speed  
44 (Figure 10f) can also be used to infer, empirically, what the maximum surface gust would  
45 approximately be *should rapid cyclogenesis ensue*. Cyclone database data (Hewson, 1998b) and  
46 subsequent experience suggest that multiplying this value by 0.5 can give a good guide. Similarly,  
47 the parameter also acts as a useful alarm bell for forecasters to occasions when the behaviour of the  
48 feature in question can be more prone to error. Recall, for example, that the cyclonic storms Lothar  
49 and Martin that hit France in December 1999 developed in the presence of very strong upper jets  
50 (Ulbrich *et al*, 2001, and Wernli *et al*, 2002), and were not well predicted by most operational  
51 models. As all the parameters depicted typically exhibit less bias than 10 m wind, they are one way  
52 in which the feature-based approach is able to address some of the deficiencies of the lower  
53 resolution ensemble forecast models, and provide useful information on the potential of a feature to  
54 cause high-impact weather.  
55  
56  
57  
58  
59  
60

1  
2 Verification data are added automatically (and of course retrospectively) to feature plumes using  
3 detection and tracking applied to model analysis fields (Figure 10, in black). On this occasion the  
4 true track and intensity are well within the spread of the ensemble. The ensemble would thus have  
5 given useful guidance to forecasters that a cyclonic feature was very likely to deepen rapidly, and  
6 that, as a result, gale-force winds could be experienced over the UK during New Year's Eve.  
7  
8

9 Note that on many manually-analysed synoptic charts occlusions are commonplace; e.g. Figures 9a,  
10 9c and 9d. Whilst this is a subtle point of departure compared to stage 6 of the conceptual model  
11 portrayed on Figure 1, it is not one that disrupts the objective identification, nor the tracking of  
12 systems. For example note how the low near Iceland on Figure 9a is successfully identified as a  
13 barotropic low on Figure 9b, and also how the arrowed frontal wave that has occluded by 0000  
14 UTC 1<sup>st</sup> (Figure 9d) is tracked well past this point (Figure 10). Indeed it is often a moot point as to  
15 where on a given chart sequence any particular warm and cold fronts should be made to evolve into  
16 occlusions (and vice versa).  
17  
18

19  
20 At longer forecast ranges storm track strike probability maps show for the user the percentage of  
21 members predicting a cyclonic feature of a set severity to track within 300 km in a certain period.  
22 Figure 11, for example, shows the probability that a feature with the potential to cause surface wind  
23 gusts greater than 60 knots would pass by during the 24-hour period when the aforementioned New  
24 Year's Eve storm hit the UK. Even at leads of 14, 11 and 8 days (Figures 11a, 11b and 11c) 30-  
25 40% of members were consistently showing a strong storm near the north of the UK. By 6 days out  
26 (Figure 11d) the probability had increased, with half the members then taking a very vigorous  
27 feature across the UK, somewhat further south. Thereafter the probability continued increasing; at  
28 4 days out (Figure 11e) it reached 80% and by 2 days (Figure 11f) out almost all members were  
29 indicating a risk for northern parts. For a more detailed analysis of this case see Titley *et al* (2008).  
30  
31

32  
33 These North Atlantic-based products from the MOGREPS ensemble have been available in real  
34 time to Met Office forecasters since late 2006. Interest from the international community has also  
35 resulted in the system being implemented at ECMWF to run on the VAREPS (Variable Resolution  
36 Ensemble Prediction System; described in Buizza *et al*, 2007).  
37

38  
39 The 'feature-based product suite' can also be adapted to work on other domains. A North Pacific  
40 suite, that also encompasses the tropics, was implemented in 2008. Products from this were made  
41 more widely available in real-time during two multi-national experiments, 'summer T-PARC' in  
42 summer and autumn of 2008, and 'winter T-PARC' in early 2009 ('T-PARC' stands for  
43 'THORPEX Pacific Asian Regional Campaign'). The overarching aim in each case was to improve  
44 predictive skill for high impact weather events. Summer T-PARC primarily focussed on tropical  
45 cyclones, on their extra-tropical transition, and on the downstream impact on medium-range  
46 forecast skill. The diagnostic tools described can be very useful in these scenarios, as illustrated by  
47 the example in Figure 12, where the barotropic low identification mechanism has correctly  
48 identified two tropical cyclone centres, and where tracking has then followed one of these through  
49 extra-tropical transition.  
50  
51

52  
53 This section has illustrated how the new cyclone identification and tracking techniques have  
54 enabled a wide range of different but related products to be developed for real time use by  
55 operational forecasters. A key element has been the application to ensemble systems, which  
56 produce far too much data for a forecaster to analyse manually. For forecaster-oriented advice on  
57 how to use such products together in an operational setting, the reader is referred to Hewson  
58 (2009b).  
59  
60

## 8. Summary

The connection between cyclonic features in the atmosphere and hazardous weather has, since the early 1900s, motivated forecasters to identify, mark and track those features. Although this remains a very valuable practice it is nonetheless costly and time-consuming, even if just a few time frames from one model sequence are considered. Nowadays, with the advent of the ‘poor man’s ensemble’ (deterministic runs from many centres), single model ensembles, multi-model ensembles, climate runs, climate ensembles and even multi-model climate ensembles, the frame count can increase by as much as six orders of magnitude, turning the processing into a breathtakingly large task, fit only for automatic computation. It is true that automated identification and tracking have been advocated for many years. However in previous studies the algorithms have tended to follow vorticity maxima or mean sea level pressure minima, when in reality cyclonic features are often centred on fronts, can take on many different forms, and regularly evolve from one type to another. Moreover, in past studies the resolution of the input data is often upscaled beforehand, to a level far greater than the 20-50 km commonly found today in both global forecast models and regional climate models. It would thus seem timely to now recognize the full range of synoptic-scale cyclonic features that the atmosphere can cast forth, and to aim to identify and track them all. Only by doing this can we really hope to account for all hazardous weather events attributable to cyclone activity, and indeed properly evaluate the potential impact of climate change thereupon.

This paper thus set out to develop a comprehensive, new and very different set of techniques for identifying and tracking cyclonic features in models. These new methods have their roots in synoptic practice, and thus retain a very real connection with the operational forecasting world, where anticipation of hazardous weather has always been a clear priority.

The paper was divided up into three topic areas, feature detection, feature tracking and applications. Key points in each area were as follows:

### Detection:

- The aim from the outset was to track cyclonic features in accordance with synoptic practice; with this in mind a pre-existing, well-known conceptual model of cyclone development was adopted (Shapiro and Keyser, 1990). This was then modified, by appending stages to the start and the end, to try to capture the *full* life-cycles of cyclonic features in the extra-tropics. Two versions of the revised model were displayed, to contrast developments on cold and warm fronts.
- The revised conceptual model provided the backbone for the objective detection techniques being developed. Three feature types were embraced: diminutive frontal waves, frontal waves and (barotropic) lows. Each required a different identification methodology.
- Detection relied on use of graphical devices, in conjunction with model-derived diagnostic fields. For the graphical post-processing, which differed greatly from previous work, we coined the term ‘the intersecting contours method’. This was because feature points are essentially detected where zero contours from two diagnostic fields intersect.
- Successful detection depends on selecting appropriate sets of diagnostics for each feature type. New sets were introduced for diminutive wave tips and for (barotropic) low centres, their behaviour being illustrated with examples. The set for frontal wave tips had been published previously.
- The detection mechanism is a ‘hybrid’, which accounts for both low-level vorticity maxima and mean sea level-pressure minima. The diminutive wave and frontal wave feature types relate to the former, barotropic lows to the latter. Only one other true ‘hybrid’ technique could be found in the literature.

- The vorticity aspect is handled in a way that differs from all previous studies. Using an objective front definition, the low-level wind field is partitioned into front-parallel and front-normal wind components, which in turn enables the vorticity itself to be partitioned, into frontal vorticity and disturbance vorticity. Feature detection then uses the disturbance vorticity, computed from front-normal (geostrophic) wind components.
- The vorticity partitioning approach possesses synoptic realism, and nicely circumvents well-documented difficulties arising when one tries to locate and track local maxima in the full vorticity field, which is often strip-like in nature, particularly near to fronts.
- Another difference in our techniques is that we require that frontal waves and diminutive waves be situated on the objectively diagnosed fronts. This too is synoptically and dynamically realistic.
- Use of a hybrid technique, whilst very powerful, introduces issues itself relating to overlapping definitions. We thus use post-processing to remove unwanted duplicates. The basis for this is a cyclone type hierarchy that has frontal waves at the top and diminutive waves at the bottom.
- Our wholly new approach to detection has meant that we can successfully and meaningfully identify features in model data of high spatial resolution (down to 50 km or so). Other studies have generally had to use downscaled data with a resolution of several hundred km.
- The integrity and synoptic utility of the objective detection techniques were tested out by comparing with features plotted subjectively, by an operational forecaster, on almost 1000 charts. When some inevitable discrepancies were allowed for the hit rate was 84% and the false alarm ratio 17%.

### Tracking:

- As the coupling of our detection mechanism to a pre-existing tracking algorithm had caused some problems we sought to develop our own tailored tracker.
- Timeliness constraints of operations meant that the data time interval could be no less than 12 h. This is twice the interval commonly used, and successful tracking, at high spatial resolution, with the large number of features we were identifying, constituted a substantial challenge.
- It became necessary to devise a relatively sophisticated feature tracking scheme, to connect root features at one time with appropriate candidate features at the next.
- First we estimate future positions of root features using a steering wind (at 500 mb) and any previous feature movement. Then we backtrack the candidate features, using just a steering wind. The idea is that the most suitable matches will ‘meet in the middle’, half way between data times. This was a new approach, which we called ‘half-time tracking’. Previous studies have used either ‘nearest neighbour searches’ with no movement estimates, or ‘full-time tracking’ in which only the root features are moved.
- Theoretical considerations suggest, encouragingly, that half-time tracking can potentially give more reliable association than full-time tracking, even when full-time tracking is applied with the inter-frame time interval halved.
- Matching was further refined by using two parameters in addition to half-time separation, one to represent feature type transition probabilities (defined using a manual training period), the other being 1000-500 hPa thickness change.
- In devising the tracker special attention was paid to ensuring that the often atypical behaviour of cyclonic windstorms was successfully catered for, to ensure that these important features would not be accidentally discarded.
- In a simple test the association failure rate for the new tracker was only 2%. This was partly because forecaster feedback on real-time products had been utilized during development.

- Tracks derived are generally smooth and continuous. This is because the contouring algorithm used during detection, implicit in the ‘intersecting contours method’, pinpoints features with a precision that is higher than the spatial resolution of the input data. It is likely that the tracking also benefits from this.

### Applications:

- The detection and tracking algorithms have been applied to the Met Office MOGREPS ensemble system to provide forecasters with useful web-based feature-related products in real-time. This is necessary because ensembles produce far too much data for the forecaster to analyse manually.
- The products are wide ranging, and were illustrated with several examples.
- At shorter leads the forecaster can click on a cyclonic feature marked on an automated control-run synoptic chart, and in so doing bring up a 6-up plot that shows the track of that feature in all members, as well as feature-specific plumes of various measures relating to modelled intensity, or potential intensity.
- At longer leads, where feature cross-referencing is less meaningful, the strategy changes, and strike probability plots, for cyclones reaching differing intensity thresholds, are provided instead.
- Various types of postage stamp plots and animations, and objective front spaghetti plots complete the product range.
- Examples depicted severe weather events, primarily windstorms, and showed how the products were able to successfully represent the causal features, and at the same time provide uncertainty information in a ‘synoptic language’ that the forecaster can recognize and utilize.

This paper concludes with reference to likely future applications of the methodology. Though primarily designed at the outset for use in the extratropics, the inclusion of ‘barotropic low’ detection enables cyclonic features in the tropics to also be identified and tracked (as on Figure 12). Evidence from the T-PARC campaign suggests that, in general, features whose intensity is greater than or equal to ‘tropical depression’ will be successfully located. This ability to track tropical cyclones makes the methodology suitable for analysing the important extra-tropical transition (‘ET’) problem (see Jones *et al*, 2003). It also opens the door to construction of a global climatology of all types of synoptic scale cyclonic feature, from minor diminutive waves on fronts, whose influence might extend 50-100 km, to very large, intense hurricanes, whose influence might reach beyond 1500 km. Indeed there are now plans to apply the techniques to reanalysis data to provide such a dataset (e.g. ERA-40 (Uppala *et al*, 2005), or the follow-up ‘ERA-interim’). When combined with feature attribute extraction and storage (similar to Hewson, 1998b) this would provide a new and valuable research resource for systematic study of cyclones at high resolution. To further improve the tracking accuracy, the intention in such studies will be to use data with a 6h or even 3h temporal resolution. Examples using 3h data in Hewson (2009a) affirm the validity of this approach.

When methods are applied to a large set of forecasts or hindcasts, opportunities arise to define model biases in terms of their impact on the ‘cyclone spectrum’ (as in Hewson, 2002) and now also on cyclones’ evolutionary history, using the tracking aspect developed since that study. Froude (2009) provides extensive results of this type obtained using the Hodges’ methodology. One-off deterministic or ensemble forecasts of high profile cyclones can also be verified in a similar way, and viewed in the context of any overall model bias.

1  
2 In the general field of model verification there is now a strong drive to develop more user-oriented  
3 measures, with a focus on severe weather (Marbouty, 2008). Consider for example an eastward  
4 moving winter-time cyclone in Europe, with heavy snow on its northern flank, heavy rain near the  
5 track, and severe winds to the south. Lateral track position determines the ‘hazard swathes’, and  
6 therefore what phenomena, if any, a given location will experience, whilst along-track errors tend  
7 to merely affect time of onset and are thus much less important (as with hurricanes). Classical  
8 measures such as root mean square error intrinsically give equal weight to both along- and cross-  
9 track errors, heavily penalizing slight timing errors, and so are not very user-oriented. Cross-track  
10 error however is clearly a much more relevant measure, and this can be readily computed wherever  
11 the current paper’s methodology is applied (using cyclone tracks from model analysis sequences as  
12 truth - note the verifying data plotted on Figure 10). Note also that routine verification of strike-  
13 probability charts (e.g. Figure 11), using for example the Brier Skill Score, intrinsically gives more  
14 weight to cross-track errors than to along-track errors; this can be particularly useful for ensemble  
15 verification. For further discussion of some verification issues see Froude (2009) and references.  
16  
17  
18  
19

20 Application to climate change simulations, and comparison with control runs or re-analysis  
21 climatology, can enable the impact of global warming on cyclonic activity to be thoroughly  
22 documented. For government and planners this should help provide clearcut, reliable signals to  
23 resolve the somewhat contradictory indications yielded to date by other studies (see Ulbrich *et al*,  
24 2009, for discussion).  
25  
26

27 Using the methodology presented in this paper it is evidently now possible to explore all the above  
28 areas using input data at 50 km resolution. A trend towards higher resolution modelling is expected  
29 to continue worldwide; late in 2009, for example, ECMWF plans to increase the resolution of its  
30 global ensemble to 32 km (up to day 10). The ‘synoptic scales’, which our methods were designed  
31 to work with, do not really extend below about 50 km, so to track features in output from such  
32 models an upscaling to the 50 km scale is considered appropriate.  
33  
34

35 In conjunction with high density observations, from radar for example, high resolution models are  
36 now highlighting relatively new types of cyclonic feature, that possess length scales of 25 km or  
37 less. The ‘misocyclones’ in Smart and Browning (2009), connected to a narrow cold frontal  
38 rainband, are one example. One would expect that in future other such classes will emerge, and that  
39 these ‘cyclonic meso-features’ will be routinely followed using new tracking algorithms, applied to  
40 data at intervals of 1h or less. At the same time focus on interactions between these new features  
41 and the synoptic-scale features discussed and tracked in this paper is expected to grow. So it seems  
42 that feature tracking technology, in various forms, can play a pivotal role here, in both research and  
43 operational contexts. Ultimately, forecasts of the associated adverse weather should improve as a  
44 result.  
45  
46  
47  
48

## 49 Appendix

### 50 Half-time tracking

51  
52  
53  
54 ‘Half-time tracking’ first uses system velocity estimates to advance a root feature R (at T0) by one  
55 half of a time step, and to retreat all candidate C features (at T1) by one half of a time step, and then  
56 delivers all the resulting half-time R-C separation distances ( $d_n$  on Figure 7) into a feature  
57 association process. This is a new approach. Full-time tracking, adopted in some previous studies,  
58 uses a system velocity estimate to instead advance R by one full time step, and then delivers the  
59 distance from this to all the true C feature positions at ‘full-time’ (i.e. T1). One way to evaluate the  
60 relative merit of half-time tracking is to consider idealized but synoptically realistic settings in

which the system velocity profile of one feature is defined a priori. Instantaneous values from this profile can then give tracking-method-related estimates of the feature's future and previous positions as appropriate, to compare with its known positions. The test is to then compare the distance between known and estimated positions, in the half-time and full-time tracking scenarios. This distance will be called the 'association error', and is clearly a function of tracking method. Naturally the larger the association error is for the true feature the more likely it is that an incorrect association (with another feature) would be made in a real-world situation. So optimal tracking would have a zero association error. Here four idealized cases will be briefly discussed, introducing the most complex one first to illustrate the principles.

**a) Case 1 – system moves 60° along a circular arc, reducing its speed linearly by 50%**

This case simulates when a feature enters the developmental left exit region of an upper level jet, and is illustrated in Figure A1. The estimated feature positions at half-time are denoted by A (forward tracking) and B (backward tracking). The half-time tracking association error is then the distance  $l_{H(T_0-T_1)}$ . This compares with the full-time tracking association error  $l_{F(T_0-T_1)}$ . Clearly the half-time tracking gives much better association; indeed the ratio of these two lengths, computed using simple trigonometry, is about 0.27.

**b) Case 2 – system moves 90° along a circular arc, with constant speed**

Half-time tracking benefits considerably from knowing that the direction of movement has changed, unlike the full-time tracking. Simple trigonometry (not shown) indicates that the association error ratio, for half-time to full-time tracking scenarios, is again about 0.27.

**c) Case 3 – system moves in a constant direction, speed varies linearly**

The half-time tracking method benefits from knowing the system acceleration (+ve or -ve). Because this is uniform, the association error for half time tracking is zero. For full time tracking it is non-zero. The association error ratio is thus 0.

**d) Case 4 – constant system velocity**

This is a trivial case in which the association error is zero in both scenarios, meaning that half-time tracking and full-time tracking are equally valid.

The above illustrates that for all but the most trivial of cases half-time tracking should provide significantly more reliable association than full time tracking. Moreover, if one were to use twice as many time frames (i.e. halving the time interval), and apply full-time tracking to those, the association error would still be *equal to or greater than* it is for half-time tracking with the full time interval. This holds for all cases. For case 1 it is illustrated on Figure A1; compare distance  $l_{H(T_0-T_1)}$  with  $l_{F(T_0-T_1/2)}$  – the ratio of these is about 0.9.

### **Acknowledgements**

Thanks to Erik Andersson and Richard Swinbank for helpful comments on an earlier draft of the paper. Thanks also to the two referees for their useful input.

## References

- Ayrault F, Joly A. 2000. L'origine des dépressions météorologiques sur l'atlantique: nouvelle perspective climatologique. *Compte-Rendus à l'Académie des Sciences, Sciences de la Terre et des planètes* **330**: 173-178.
- Benestad R, Chen D. 2006. The use of a calculus-based cyclone identification method for generating storm statistics. *Tellus Series A-Dynamic Meteorology and Oceanography* **58**: 473-486.
- Bengtsson L, Hodges KI, Keenlyside N. 2009. Will extratropical storms intensify in a warmer climate? *Journal of Climate* **22**: 2276-2301.
- Berry G, Thorncroft C, Hewson T. 2007. African easterly waves during 2004—analysis using objective techniques. *Monthly Weather Review* **135**: 1251-1267.
- Blender R, Schubert M. 2000. Cyclone tracking in different spatial and temporal resolutions. *Monthly Weather Review* **128**: 377-384.
- Bowler NE, Arribas A, Mylne KR, Robertson KB, Beare SE. 2008. The MOGREPS short-range ensemble prediction system. *Quarterly Journal of the Royal Meteorological Society* **134**: 703-722.
- Bracegirdle TJ, Gray SL. 2007. An objective climatology of the dynamical forcing of polar lows in the Nordic seas. *International Journal of Climate* **14**: 1903-1919.
- Buizza R, Bidlot JR, Wedi N, Fuentes M, Hamrud M, Holt G, Vitart F. 2007. The new ECMWF VAREPS (Variable Resolution Ensemble Prediction System). *Quarterly Journal of the Royal Meteorological Society* **133**: 681-695.
- Chen Q-s, Bromwich DH. 1999. An equivalent isobaric geopotential height and its application to synoptic analysis and a generalized omega-equation in sigma coordinates. *Monthly Weather Review* **127**: 145-172.
- Dacre HF, Gray SL. 2009. The spatial distribution and evolution characteristics of North Atlantic cyclones. *Monthly Weather Review* **137**: 99-115.
- Deveson ACL, Browning KA, Hewson TD. 2002. A Classification of FASTEX cyclones using a height-attributable QG vertical motion diagnostic. *Quarterly Journal of the Royal Meteorological Society* **128**: 93-117.
- Froude LSR. 2009. Regional differences in the prediction of extratropical cyclones by the ECMWF ensemble prediction system. *Monthly Weather Review* **137**: 893-911.
- Geng Q, Sugi M. 2001. Variability of the North Atlantic cyclone activity in winter analyzed from NCEP–NCAR reanalysis data. *Journal of Climate* **14**: 3863–3873.
- Gray SL, Dacre HF. 2006. Classifying dynamical forcing mechanisms using a climatology of extratropical cyclones. *Quarterly Journal of the Royal Meteorological Society* **132**: 1119-1137.
- Hanson CE, Palutikof JP, Davies TD. 2004. Objective cyclone climatologies in the North Atlantic – a comparison between the ECMWF and NCEP reanalyses. *Climate Dynamics* **22**: 757-769.

- 1  
2 Hewson TD. 1997. Objective identification of frontal wave cyclones. *Meteorological Applications*  
3 **4**: 311-315.  
4  
5  
6 Hewson TD. 1998a. Objective fronts. *Meteorological Applications* **5**: 37-65.  
7  
8 Hewson TD. 1998b. A frontal wave database. JCMM Internal Report No. 85. pp 20. Department of  
9 Meteorology, University of Reading.  
10  
11 Hewson TD, Craig GC, Claud C. 2000. A polar low outbreak: Evolution and mesoscale structures.  
12 *Quarterly Journal of the Royal Meteorological Society* **126**: 1031-1063.  
13  
14  
15 Hewson TD. 2001. The North Sea storm of 30 October 2000. *Weather* **56**: 115-116.  
16  
17  
18 Hewson TD. 2002. A comparison of cyclone spectra in forecasts from the operational (G1) and new  
19 dynamics trial (NT) versions of the unified model – Aug to Dec 2001. Met Office Forecasting  
20 Research Technical Report No. 376. Met Office, Exeter, UK.  
21  
22  
23 Hewson TD. 2009a. Diminutive frontal waves—A link between fronts and cyclones. *Journal of the*  
24 *Atmospheric Sciences* **66**: 116-132.  
25  
26  
27 Hewson TD. 2009b. Tracking fronts and extra-tropical cyclones. *ECMWF newsletter* **121**: 9-19.  
28  
29  
30 Hodges KI. 1994. A general method for tracking analysis and its application to meteorological data.  
31 *Monthly Weather Review* **122**: 2573-2586.  
32  
33  
34 Hodges KI. 1995. Feature tracking on the unit sphere. *Monthly Weather Review* **123**: 3458-3465.  
35  
36  
37 Hodges KI. 1996. Spherical nonparametric estimators applied to the UGAMP model integration for  
38 AMIP. *Monthly Weather Review* **124**: 2914-2932.  
39  
40  
41 Hoskins BJ, 1982. The Mathematical Theory of Frontogenesis. *Annual Review of Fluid Mechanics*.  
42 **14**: Pages 131-151.  
43  
44  
45 Hoskins BJ, Hodges KI. 2002. New perspectives on the Northern Hemisphere winter storm tracks.  
46 *Journal of the Atmospheric Sciences* **59**: 1041-1061.  
47  
48  
49 Jones SC, Harr PA, Abraham J, Bosart LF, Bowyer PJ, Evans JL, Hanley DE, Hanstrum BN, Hart  
50 RE, Lalaurette F, Sinclair MR, Smith RK, Thorncroft C. 2003. The extratropical transition of  
51 tropical cyclones: Forecast challenges, current understanding, and future directions. *Weather and*  
52 *Forecasting* **18**: 1052-1092.  
53  
54  
55 Kleppek S, Muccione V, Raible CC, Bresch DN, Koellner-Heck P, Stocker TF. 2008.  
56 Tropical cyclones in ERA-40: A detection and tracking method. *Geophysical Research Letters* **35**:  
57 L10705.  
58  
59  
60 König W, Sausen R, Sielmann F. 1993. Objective identification of cyclones in GCM simulations.  
*Journal of Climate* **6**: 2217-2231.  
  
Lalaurette F. 2003. Early detection of abnormal weather conditions using a probabilistic extreme  
forecast index. *Quarterly Journal of the Royal Meteorological Society* **129**: 3037-3057.

- 1  
2 Legg TP, Mylne KR. 2004. Early warnings of severe weather from ensemble forecast information.  
3 *Weather and Forecasting* **19**: 891-906.  
4
- 5 Marbouty D. 2008. Editorial - Early warning of severe weather. *ECMWF Newsletter* **117**: 1.  
6  
7
- 8 Mass CF. 1991. Synoptic frontal analysis: Time for a reassessment? *Bulletin of the American*  
9 *Meteorological Society* **72**: 348-363.  
10
- 11 McCallum E. 1990. The Burns' Day Storm, 25 January 1990. *Weather* **45**: 166-173.  
12
- 13 Murray RJ, Simmonds I. 1991. A numerical scheme for tracking cyclone centres from digital data.  
14 Part I: development and operation of the scheme. *Australian Meteorological Magazine* **39**: 155-  
15 166.  
16  
17
- 18 Petterssen S, Smebye SJ. 1971. On the development of extratropical cyclones. *Quarterly Journal of*  
19 *the Royal Meteorological Society* **97**: 457-482.  
20  
21
- 22 Pinto JG, Spanghel T, Ulbrich U, Speth P. 2005. Sensitivities of a cyclone detection and tracking  
23 algorithm: individual tracks and climatology. *Meteorologische Zeitschrift* **14**: 823-838.  
24
- 25 Plant RS, Craig GC, Gray SL. 2003. On a three-fold theory of extratropical cyclogenesis. *Quarterly*  
26 *Journal of the Royal Meteorological Society* **129**: 2989-3012.  
27  
28
- 29 Raible CC, Della-Marta PM, Schwierz C, Wernli H, Blender R. 2008. Northern Hemisphere  
30 extratropical cyclones: A comparison of detection and tracking methods and different reanalyses.  
31 *Monthly Weather Review* **136**: 880-897.  
32  
33
- 34 Renfrew IA, Thorpe AJ, Bishop CH. 1997. The role of the environmental flow in the development  
35 of secondary frontal cyclones. *Quarterly Journal of the Royal Meteorological Society* **123**: 1653-  
36 1675.  
37  
38
- 39 Serreze MC, Carse F, Barry RG, Rogers JC. 1997. Icelandic low cyclone activity: Climatological  
40 features, linkages with the NAO, and relationships with the recent changes in the northern  
41 hemisphere circulation. *Journal of Climate* **10**: 453-464.  
42
- 43 Shapiro MA, Keyser D. 1990. Fronts, jet streams and the tropopause. In *Extratropical Cyclones,*  
44 *The Erik Palmén Memorial Volume*, Newton CW, Holopainen EO (eds.). American Meteorological  
45 Society; 167-191.  
46  
47
- 48 Sickmüller M, Blender R, Fraedrich K. 2000. Observed winter cyclone tracks in the Northern  
49 Hemisphere in re-analysed ECMWF data. *Quarterly Journal of the Royal Meteorological Society*  
50 **126**: 591-620.  
51  
52
- 53 Simmonds I, Murray RJ, Leighton RM. 1999. A refinement of cyclone tracking methods with data  
54 from FROST. *Australian Meteorological Magazine* (Special ed.): 35-49.  
55
- 56 Simmonds I, Murray RJ. 1999. Southern extratropical cyclone behaviour in ECMWF analyses  
57 during the FROST special observing periods. *Weather and Forecasting* **14**: 878-891.  
58  
59
- 60 Sinclair MR. 1994. An objective cyclone climatology for the Southern Hemisphere. *Monthly*  
*Weather Review* **122**: 2239-2256.

1  
2  
3 Smart DJ, Browning KA. 2009. Morphology and evolution of cold-frontal misocyclones. *Quarterly*  
4 *Journal of the Royal Meteorological Society* **135**: 381-393.

5  
6  
7 Terry J, Atlas R. 1996. Objective cyclone tracking and its application to ERS-1 scatterometer  
8 forecast impact studies. 15th Conference on Weather Analysis and Forecasting, Norfolk, VA.  
9 American Meteorological Society; 146-149.

10  
11 Titley HA, Savage N, Swinbank R, Thompson S. 2008. Comparison between Met Office and  
12 ECMWF medium-range ensemble forecast systems. Met Office Forecasting Research Technical  
13 Report No. 512. Met Office, Exeter, UK.

14  
15  
16 Ulbrich U, Fink AH, Klawe M, Pinto JG. 2001. Three extreme storms over Europe in December  
17 1999. *Weather* **56**: 70-80.

18  
19  
20 Ulbrich U, Leckebusch GC, Pinto JG. 2009. Extra-tropical cyclones in the present and future  
21 climate: a review. *Theoretical and Applied Climatology* **54**: 139-146.

22  
23 Uppala SM, Co-authors. 2005. The ERA-40 re-analysis. *Quarterly Journal of the Royal*  
24 *Meteorological Society* **131**: 2961-3012.

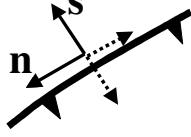
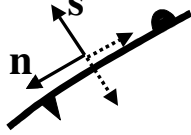
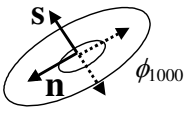
25  
26  
27 Watkin HA, Hewson TD. 2006. The development of feature-based diagnostics to assess TIGGE  
28 handling of high-impact extra-tropical cyclones. Extended abstracts, 2nd THORPEX International  
29 Science Symposium, Landshut, Germany. World Meteorological Organisation; 258-259.

30  
31  
32 Wernli H, Dirren S, Liniger MA, Zillig M. 2002. Dynamical aspects of the life-cycle of the winter  
33 storm 'Lothar' (24-26 December 1999). *Quarterly Journal of the Royal Meteorological Society*  
34 **128**: 405-429.

35  
36  
37 Wernli H, Schwierz C. 2006. Surface cyclones in the ERA40 data set (1958-2001). Part I: novel  
38 identification method and global climatology. *Journal of the Atmospheric Sciences* **63**: 2486-2507.

39  
40  
41 Zolina O, Gulev SK. 2002. Improving the accuracy of mapping cyclone numbers and frequencies.  
42 *Monthly Weather Review* **130**: 748-759.

43  
44  
45 Zsótér E. 2006. Recent developments in extreme weather forecasting. *ECMWF newsletter* **107**: 8-  
46 17.

CYCLONIC FEATURE	DIAGNOSTIC TYPE	COMMENT	EQUATION	THRESH-OLDS Standard Weak
<b>DIMINUTIVE FRONTAL WAVE</b>  <i>'A point on a front characterised by a local maximum, in the along-front direction, in the vorticity of the cross-front geostrophic wind'</i>  All variables are on the surface 'geopotential height above topography =1km'    $\hat{s}_{front} = \pm \nabla  \nabla \theta_w  /  \nabla \nabla \theta_w $ (5 point mean axis)	Locating DL1	Front locator	$\partial(\nabla  \nabla \theta_w )_s / \partial s = 0$	N/A
	Locating DL2	Turning points in an along-front profile of vorticity of the cross-front geostrophic wind	$\partial^2 V_{Gs} / \partial n^2 = 0$	N/A
	Masking DM1	Rate of change of theta-w gradient, across theta-w isotherms (front)	$-\nabla  \nabla \theta_w  \cdot \nabla \theta_w /  \nabla \theta_w  >$	0.52 °C / (100 km) <sup>2</sup> 0.26 °C / (100 km) <sup>2</sup>
	Masking DM2	Approximate theta-w gradient in the adjacent baroclinic zone (front)	$ \nabla \theta_w  + m\chi  \nabla \nabla \theta_w  >$	1.17 °C / 100 km 0.595 °C / 100 km
	Masking DM3	Approximate theta gradient in the adjacent baroclinic zone (front)	$ \nabla \theta  + m\chi  \nabla \nabla \theta  >$	1.17 °C / 100 km 0.595 °C / 100 km
	Masking DM4	Relative vorticity	$\partial v / \partial x - \partial u / \partial y >$	0
	Masking DM5	Nature of turning point in the along-front profile of vorticity of the cross-front geostrophic wind (cf. DL2)	$-\partial^3 V_{Gs} / \partial n^3 >$	0
Masking DM6	Vorticity of the cross-front geostrophic wind (= geostrophic disturbance vorticity)	$-\partial V_{Gs} / \partial n >$	$8.0 \times 10^{-6} \text{ s}^{-1}$	
<b>FRONTAL WAVE</b>  <i>'A meeting point of cold and warm fronts at which the vorticity of the cross-front geostrophic wind is positive'</i>  All variables are on the surface 'geopotential height above topography =1km'    $\hat{s}_{front} = \pm \nabla  \nabla \theta_w  /  \nabla \nabla \theta_w $ (5 point mean axis)	Locating WL1	Front locator (same as DL1)	$\partial(\nabla  \nabla \theta_w )_s / \partial s = 0$	N/A
	Locating WL2	Zero geostrophic theta-w advection	$\mathbf{V}_G \cdot \nabla \theta_w = 0$	N/A
	Masking WM1	Same as DM1	$-\nabla  \nabla \theta_w  \cdot \nabla \theta_w /  \nabla \theta_w  >$	0.52 °C / (100 km) <sup>2</sup> 0.26 °C / (100 km) <sup>2</sup>
	Masking WM2	Same as DM2	$ \nabla \theta_w  + m\chi  \nabla \nabla \theta_w  >$	1.17 °C / 100 km 0.595 °C / 100 km
	Masking WM3	Same as DM3	$ \nabla \theta  + m\chi  \nabla \nabla \theta  >$	1.17 °C / 100 km 0.595 °C / 100 km
	Masking WM4	Same as DM4	$\partial v / \partial x - \partial u / \partial y >$	0
	Masking WM5	Wave – anti-wave discriminant	$[\nabla  \nabla \theta_w  \times \hat{k}] \cdot \nabla [-\mathbf{V}_G \cdot \nabla \theta_w] >$	0
<b>'BAROTROPIC' LOW</b>    $\hat{s}_{low} = \pm \nabla \phi_{1000} /  \nabla \phi_{1000} $ (5 point mean axis)	Locating BL1	x-component of the pressure gradient	$\partial \phi_{1000} / \partial x = 0$	N/A
	Locating BL2	y-component of the pressure gradient	$\partial \phi_{1000} / \partial y = 0$	N/A
	Masking BM1	Geostrophic vorticity factor (1-2-1 filter applied 4 times)	$(\nabla^2 \phi_{1000})_{filtered} >$	$1.0 \times 10^{-9} \text{ m}^{-1}$
	Masking BM2	Col point discriminant	$\partial^2 \phi_{1000} / \partial n^2 * \partial^2 \phi_{1000} / \partial s^2 >$	0

**Table I: DEFINING EQUATIONS FOR DIFFERENT CYCLONE TYPES.** WL1, WL2, WM1, WM2 and WM5 are from Hewson (1997). Shading denotes 'pragmatic' masking (see text). Thresholds are for derivatives computed across 100km. The term 'barotropic' in 'barotropic low' reflects post-processing; it is not implicit in the equations themselves - see section 4.2.

	Cause of Discrepancy	Number of Cases	
		Misses = Synoptic Chart Feature not on Objective Chart (57 cases total)	False Alarms = Objective Chart Feature not on Synoptic Chart (20 cases total)
1	Feature just inside box on one chart, just outside on the other	6	6
2	Weak / flabby low centre	15	2
3	Objectively represented as a weak frontal wave or a standard or weak diminutive wave	12	N/A
4	Frontal wave manually plotted contrary to geostrophic flow (i.e. no evidence for warm <i>and</i> cold fronts)	4	N/A
5	Double or complex frontal structure, relating to frontal wave, not represented as such	6	0
6	Clear analysis error in model	3	0
7	Frontal wave; front completely missing from other chart	8	1
8	Flow almost parallel to front	3	11

**Table II:** REASONS FOR DISCREPANCIES BETWEEN OBJECTIVE AND SUBJECTIVE CHARTS.

**Figure Captions**

**Figure 1:** Idealised system-relative view of the life-cycles of two vigorous northern hemisphere extra-tropical cyclones, developing on a cold front (top row) and on a warm front (bottom row). Panels show isobars, primary fronts, flow direction and the notional cyclonic centre. Stages 3 to 6 are based on Shapiro and Keyser (1990) – see text. Stages 0, 1, 2 and 7 have been added. Labelling below indicates the objective identification method used to identify each stage (see Table I). Note that the objective cyclonic features are in no way constrained by this conceptual model to follow the evolutionary pathways it depicts; instead the model aims to provide an introductory framework for visualizing the types of feature the new methodology was designed to identify.

**Figure 2:** **a)** snapshot of all cyclonic features (circles) automatically detected in T+72 h model forecast fields for VT 0000 UTC 20 Sep 2004. Barotropic lows are shown in black, diminutive waves in green and frontal wave cyclones in orange (as on the panel (b) legend). Smaller circles denote weak features (i.e. those situated on objective fronts that satisfy only weak thermal gradient threshold criteria). Also shown are both standard and weak objective warm (red) and cold (blue) fronts, and mean sea level pressure (black, hPa). **b)** tracking history, within the same model forecast, at 12 h intervals, within a +/-72 h time window, for all features shown on panel (a) (except weak ones). Solid circles are from panel (a), open circles are for other times. On both panels purple highlighting relates to features discussed in Section 6.2.

**Figure 3:** Graphical processing stages – activated sequentially (only a small chart segment is shown). **a)** 1<sup>st</sup> locating diagnostic contoured. **b)** 1<sup>st</sup> masking diagnostic colour-filled (grey shading denoting transparent, white denoting white colour-fill). **c)** panel (b) overlaid on panel (a) (line segment output). **d)** 2<sup>nd</sup> locating diagnostic contoured. **e)** panel (d) transposed. **f)** panel (e) overlaid on panel (c). **g)** 2<sup>nd</sup> masking diagnostic colour-filled. **h)** panel (g) overlaid on panel (f) (point output). At processing stages corresponding to panels (b) and (g) several different masks might be computed and applied consecutively.

**Figure 4:** Met Office global model output at 900hPa for T+120h = 0000 UTC 9 Oct 2004, for an area south of Greenland. **a)** dashed black contour shows an objectively identified cold front (DL1), white contours are geopotential height. Colours show geostrophic disturbance vorticity (DM6 on Table I). Arrows and labels denote subjectively-determined along-front maxima (An) and minima (Bn) in the coloured field, clear-cut cases being denoted by solid arrows, marginal cases by dashed arrows. Solid black contours show where the along-front derivative of the disturbance vorticity is zero (DL2); blackened circles highlight intersections of locating contours DL1 and DL2 which are thus the objective counterparts of the (subjectively) labelled points. **b)** all contours are as on panel (a), whilst colours shows the second derivative, in the along-front direction, of the geostrophic disturbance vorticity (DM5).

**Figure 5:** Model output for T+36h = 1200 UTC on 5 Oct 2004. White contours show 1000 hPa geopotential height, blue contours (two sets) are zero contours for locating diagnostics BL1 and BL2. Labels highlight all blue contour intersection points. Mask BM1 is denoted by pink contours, which enclose areas where its threshold is satisfied ( $>1.0 \times 10^{-9} \text{ m}^{-1}$ , see Table I). Mask BM2 is depicted by shading, yellow through red denotes threshold satisfied ( $>0$ ). Thus X1 and X3 pass both masking tests, and so are low centres. X2 and X4 are rejected, for different reasons.

**Figure 6:** Hypothetical illustration of cyclonic feature post-processing, showing in map format pixels that denote cyclonic centres after each stage (pixels are enlarged for clarity). The legend shows meaning of the symbols, and the separation threshold used. Processing order is (a) then (b) then (c). **a)** results from graphical processing of diagnostics on Table I. **b)** results from then addressing ‘borderline cases’. **c)** results from then addressing the ‘overlap problem’; this equates to the final product. See text for further information.

**Figure 7:** An illustration of the tracking scheme association process for one root feature R. Only those candidate features  $C_i$  that passed check 1 - i.e. whose estimated half-time position lies within the dotted ring - are shown. Grey shading within features denotes feature type (see text). “Half-time” positions are estimated as follows: for R using 500 hPa winds, and previous movement if available; for all  $C_i$  using only 500 hPa winds. ‘Half-time separation’ is distance  $d_i$ . **Inset:** a pictorial representation of the least squares approach to finding the best candidate match for R, using three likelihood parameters (labelled axes). Half-time separation is one such parameter; dotted lines are vertical projections onto the horizontal plane ‘Separation=0’, and thus denote  $d_i$ . The matched candidate is generally the one closest to the origin (see dashed lines) – in this case  $C_3$ . Only if  $C_3$  were later ‘stolen’ during the iterative process that links Rs to the Cs for that time step would this not be the case (see text).

**Figure 8:** Composite “spaghetti” plot of fronts identified in all 24 MOGREPS-15 ensemble members for the T+36h forecast from DT 0000 UTC 24 April 2008, taken from a multiple lead-time animation. Cold/warm fronts are shown in blue/red for perturbed members and green/gold for the control forecast. Thermally weak fronts are omitted. Note the

1  
2  
3  
4  
5  
6  
7  
8  
9  
10  
11  
12  
13  
14  
15  
16  
17  
18  
19  
20  
21  
22  
23  
24  
25  
26  
27  
28  
29  
30  
31  
32  
33  
34  
35  
36  
37  
38  
39  
40  
41  
42  
43  
44  
45  
46  
47  
48  
49  
50  
51  
52  
53  
54  
55  
56  
57  
58  
59  
60

large spread in handling of features to the west and southwest of the UK, and relatively small spread for all other features.

**Figure 9:** Manually-analysed synoptic charts from the Met Office for 0000 UTC on 30<sup>th</sup> (a), and 31<sup>st</sup> (c) December 2006, and 1<sup>st</sup> January 2007 (d). Objectively identified fronts and cyclonic features in the MOGREPS control analysis for 0000 UTC 30th are shown in (b) - see Figure 2 for symbol meaning. Isobar interval on all panels is 4hPa. Arrows highlight the developing cyclone discussed in the text. In the web version of panel (b) the user can click on any feature spot to bring up feature-specific information such as that shown on Figure 10.

**Figure 10:** MOGREPS-15 ensemble: **a)** Forecast tracks for the key frontal wave from 0000 UTC 30 December 2006 (arrowed on Figure 9b). **b)-f)** Associated feature-specific plumes for five diagnostic measures (control=green, analysis=black). Vertical lines denote 0000 UTC on consecutive days, year change is darker. **b)** mean sea level pressure at the feature point (hPa), **c)** maximum 1 km wind within 600 km of the feature point (knots), **d)** relative vorticity at the feature point ( $\times 10^{-6} s^{-1}$ ), **e)** maximum 1 km wind within 300 km of the feature point (knots). **f)** maximum 300 hPa wind within 600 km of the feature point (knots). Tabulated data that shows, as a function of lead, the percentage of members that captured the feature, have been omitted.

**Figure 11:** MOGREPS-15 ensemble 'storm track strike probability' forecasts, from a range of lead times, for a fixed validity period of 0000-2400UTC on 31 December 2006. Colours show the probability that a cyclonic feature, that has attributed to it (i.e. within a 300km radius) a maximum 1 km wind of  $> 60$  knots, will pass within 300 km during the 24 h period. Each panel denotes a different lead time: **a)** 336h, **b)** 264h, **c)** 192h, **d)** 144h, **e)** 96h, **f)** 48h.

**Figure 12: a):** Objectively analysed fronts and features in the MOGREPS control analysis for 1200 UTC on 22 Nov 2007 (see Figure 2 for symbol meaning). Mean sea level pressure contours are at 4 hPa intervals. Two tropical cyclones have been identified: Hagibis in the South China Sea, and Mitag to the east of the Philippines. **b)** Forecast tracks for Typhoon Mitag from the same data time from the MOGREPS-15 ensemble. The storm was forecast to track over the Philippines, where it led to at least 10 fatalities, before undergoing extra-tropical transition. In the ensemble the acquisition of a frontal structure and the concurrent transition to the frontal wave cyclone class is denoted by a change from black to orange spots, and is evidently picked out well by the identification methods. This transition looks to occur in most members just after the completion of recurvature.

**Figure A1:** Idealized case of a cyclonic feature 'turning to the left', along the arc of a circle of radius  $r$ , linearly reducing its speed by 50% in  $60^\circ$ . Grey spots denote feature position at three equally spaced times. Distances  $l_{H(t)}$  and  $l_{F(t)}$  denote, respectively, the association errors for half-time tracking and full-time tracking of that feature, for frame time interval  $t$ . The figure is essentially drawn to scale, albeit with some arrows offset slightly to aid clarity.

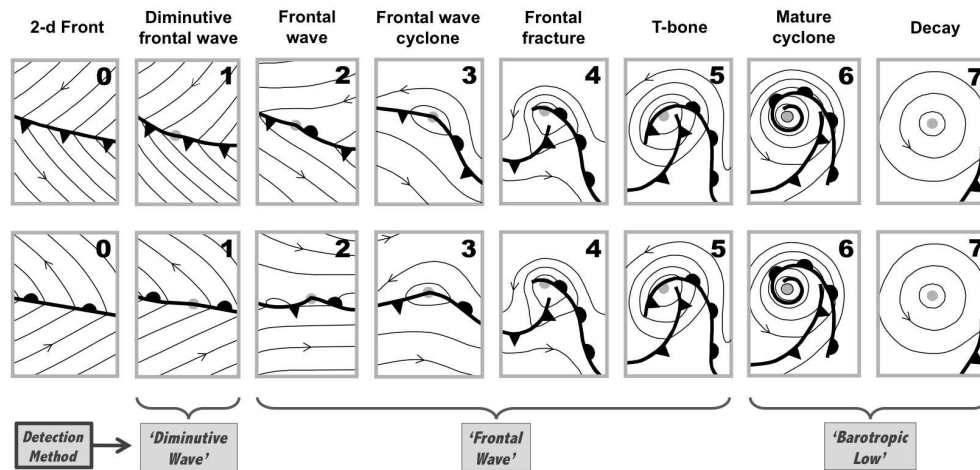


Figure 1: Idealised system-relative view of the life-cycles of two vigorous northern hemisphere extra-tropical cyclones, developing on a cold front (top row) and on a warm front (bottom row). Panels show isobars, primary fronts, flow direction and the notional cyclonic centre. Stages 3 to 6 are based on Shapiro and Keyser (1990) – see text. Stages 0, 1, 2 and 7 have been added. Labelling below indicates the objective identification method used to identify each stage (see Table I). Note that the objective cyclonic features are in no way constrained by this conceptual model to follow the evolutionary pathways it depicts; instead the model aims to provide an introductory framework for visualizing the types of feature the new methodology was designed to identify.  
580x279mm (72 x 72 DPI)

Review

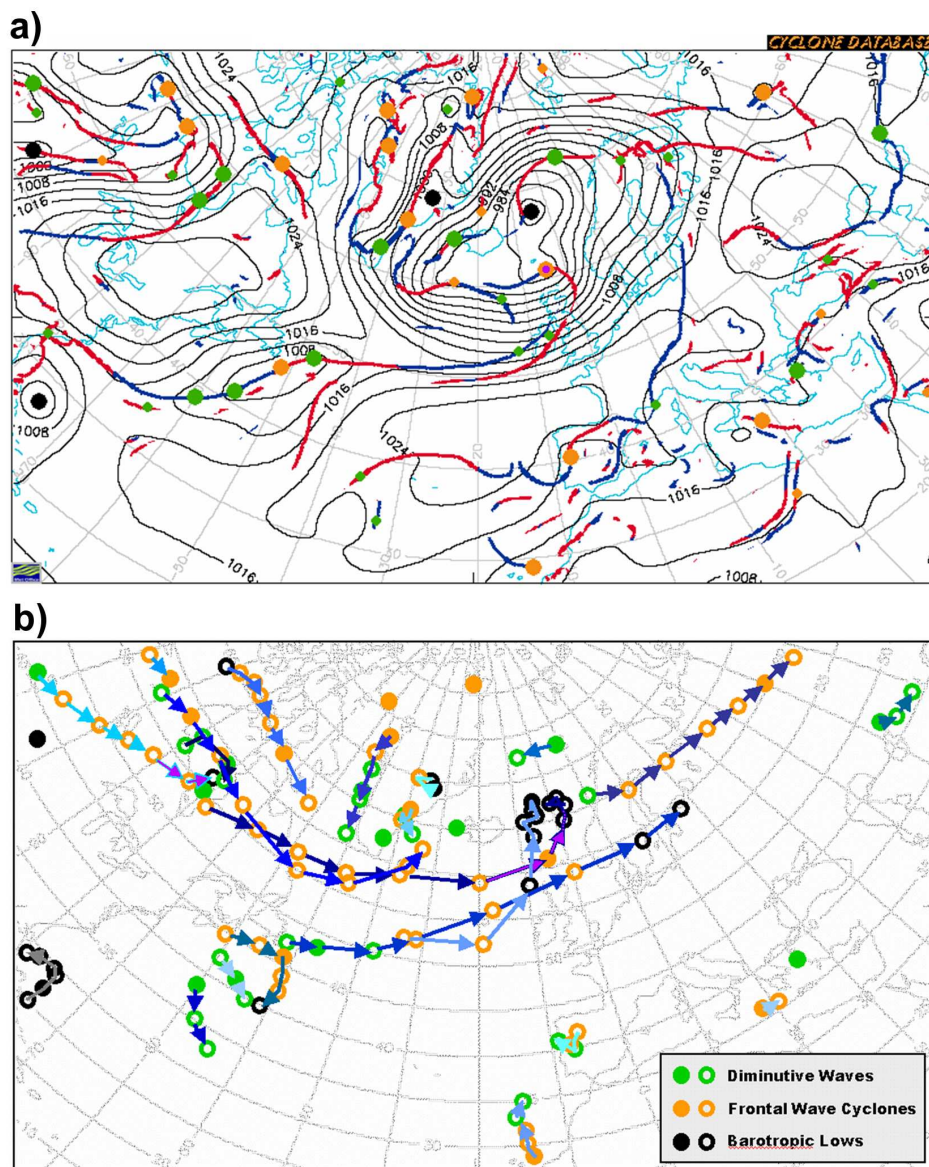


Figure 2: a) snapshot of all cyclonic features (circles) automatically detected in T+72 h model forecast fields for VT 0000 UTC 20 Sep 2004. Barotropic lows are shown in black, diminutive waves in green and frontal wave cyclones in orange (as on the panel (b) legend). Smaller circles denote weak features (i.e. those situated on objective fronts that satisfy only weak thermal gradient threshold criteria). Also shown are both standard and weak objective warm (red) and cold (blue) fronts, and mean sea level pressure (black, hPa). b) tracking history, within the same model forecast, at 12 h intervals, within a  $\pm 72$  h time window, for all features shown on panel (a) (except weak ones). Solid circles are from panel (a), open circles are for other times. On both panels purple highlighting relates to features discussed in Section 6.2.

456x559mm (96 x 96 DPI)

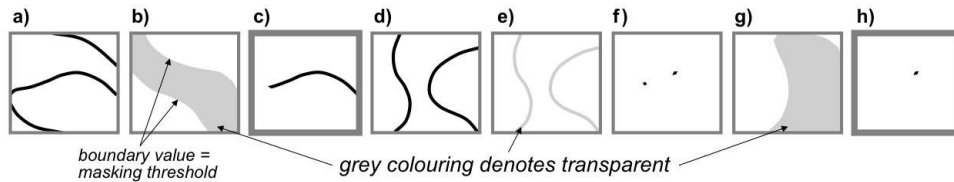


Figure 3: Graphical processing stages – activated sequentially (only a small chart segment is shown). a) 1st locating diagnostic contoured. b) 1st masking diagnostic colour-filled (grey shading denoting transparent, white denoting white colour-fill). c) panel (b) overlaid on panel (a) (line segment output). d) 2nd locating diagnostic contoured. e) panel (d) transposed. f) panel (e) overlaid on panel (c). g) 2nd masking diagnostic colour-filled. h) panel (g) overlaid on panel (f) (point output). At processing stages corresponding to panels (b) and (g) several different masks might be computed and applied consecutively.

458x88mm (72 x 72 DPI)

Peer Review

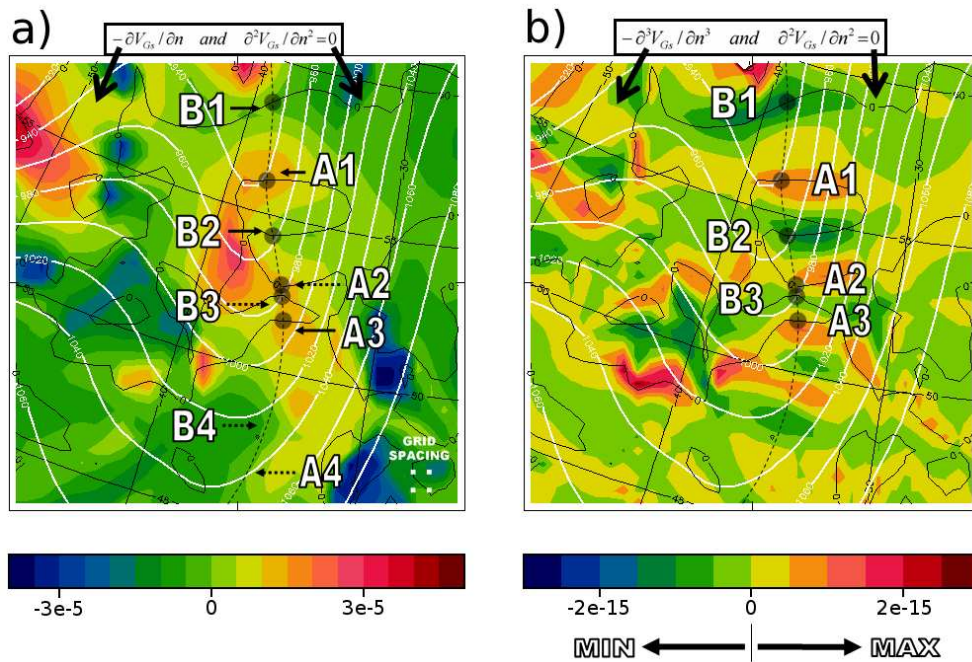


Figure 4: Met Office global model output at 900hPa for T+120h = 0000 UTC 9 Oct 2004, for an area south of Greenland. a) dashed black contour shows an objectively identified cold front (DL1), white contours are geopotential height. Colours show geostrophic disturbance vorticity (DM6 on Table I). Arrows and labels denote subjectively-determined along-front maxima (An) and minima (Bn) in the coloured field, clear-cut cases being denoted by solid arrows, marginal cases by dashed arrows. Solid black contours show where the along-front derivative of the disturbance vorticity is zero (DL2); blackened circles highlight intersections of locating contours DL1 and DL2 which are thus the objective counterparts of the (subjectively) labelled points. b) all contours are as on panel (a), whilst colours shows the second derivative, in the along-front direction, of the geostrophic disturbance vorticity (DM5).  
357x240mm (72 x 72 DPI)

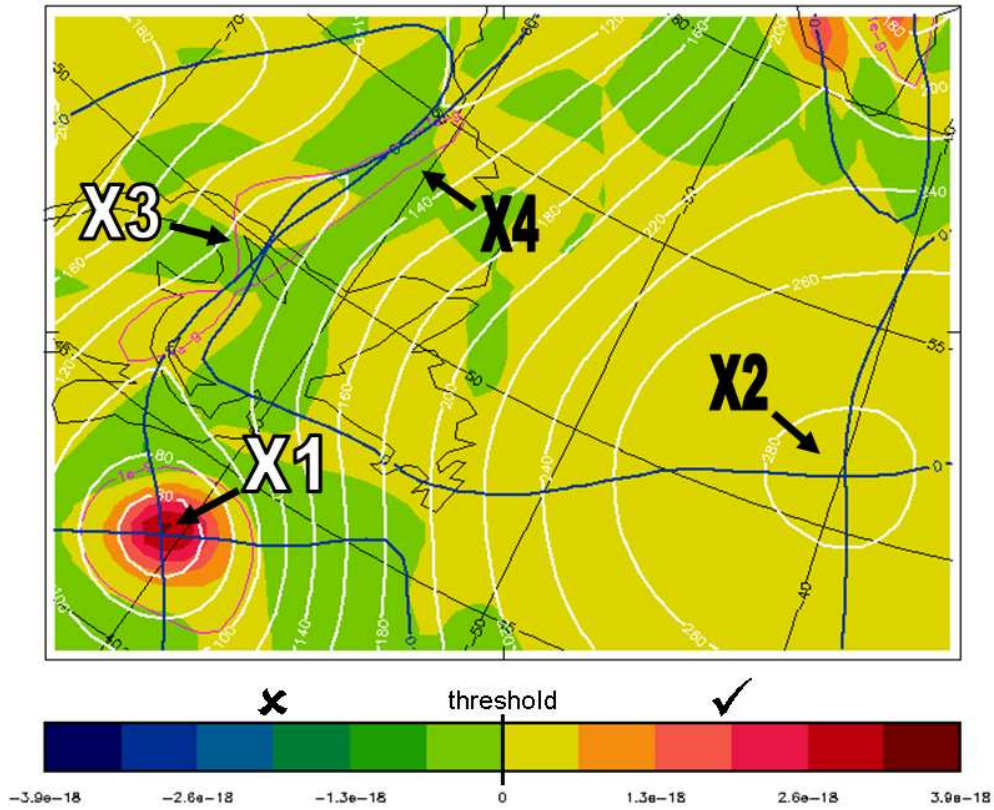
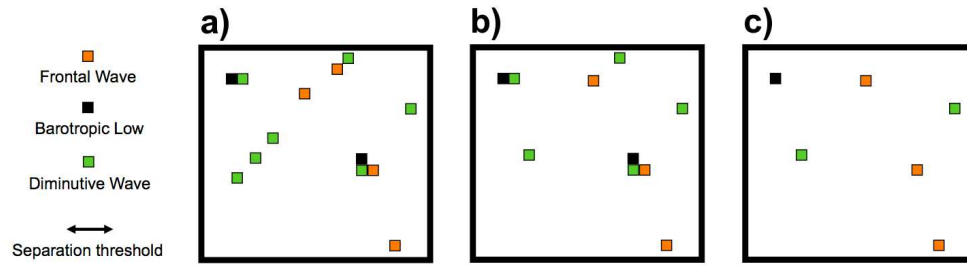


Figure 5: Model output for T+36h = 1200 UTC on 5 Oct 2004. White contours show 1000 hPa geopotential height, blue contours (two sets) are zero contours for locating diagnostics BL1 and BL2. Labels highlight all blue contour intersection points. Mask BM1 is denoted by pink contours, which enclose areas where its threshold is satisfied ( $>1.0 \times 10^{-9} \text{ m}^{-1}$ , see Table I). Mask BM2 is depicted by shading, yellow through red denotes threshold satisfied ( $>0$ ). Thus X1 and X3 pass both masking tests, and so are low centres. X2 and X4 are rejected, for different reasons.

282x229mm (72 x 72 DPI)



18 Figure 6: Hypothetical illustration of cyclonic feature post-processing, showing in map format pixels  
19 that denote cyclonic centres after each stage (pixels are enlarged for clarity). The legend shows  
20 meaning of the symbols, and the separation threshold used. Processing order is (a) then (b) then  
21 (c). a) results from graphical processing of diagnostics on Table I. b) results from then addressing  
22 'borderline cases'. c) results from then addressing the 'overlap problem'; this equates to the final  
23 product. See text for further information.

24 518x141mm (72 x 72 DPI)

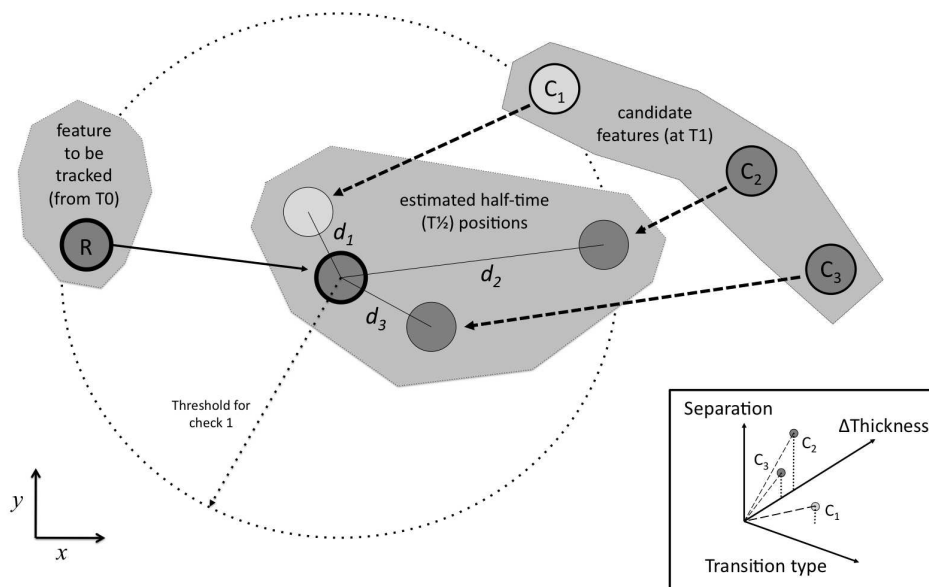


Figure 7: An illustration of the tracking scheme association process for one root feature R. Only those candidate features  $C_i$  that passed check 1 - i.e. whose estimated half-time position lies within the dotted ring - are shown. Grey shading within features denotes feature type (see text). "Half-time" positions are estimated as follows: for R using 500 hPa winds, and previous movement if available; for all  $C_i$  using only 500 hPa winds. 'Half-time separation' is distance  $d_i$ . **Inset:** a pictorial representation of the least squares approach to finding the best candidate match for R, using three likelihood parameters (labeled axes). Half-time separation is one such parameter; dotted lines are vertical projections onto the horizontal plane 'Separation=0', and thus denote  $d_i$ . The matched candidate is generally the one closest to the origin (see dashed lines) - in this case  $C_3$ . Only if  $C_3$  were later 'stolen' during the iterative process that links Rs to the Cs for that time step would this not be the case (see text).  
589x359mm (72 x 72 DPI)

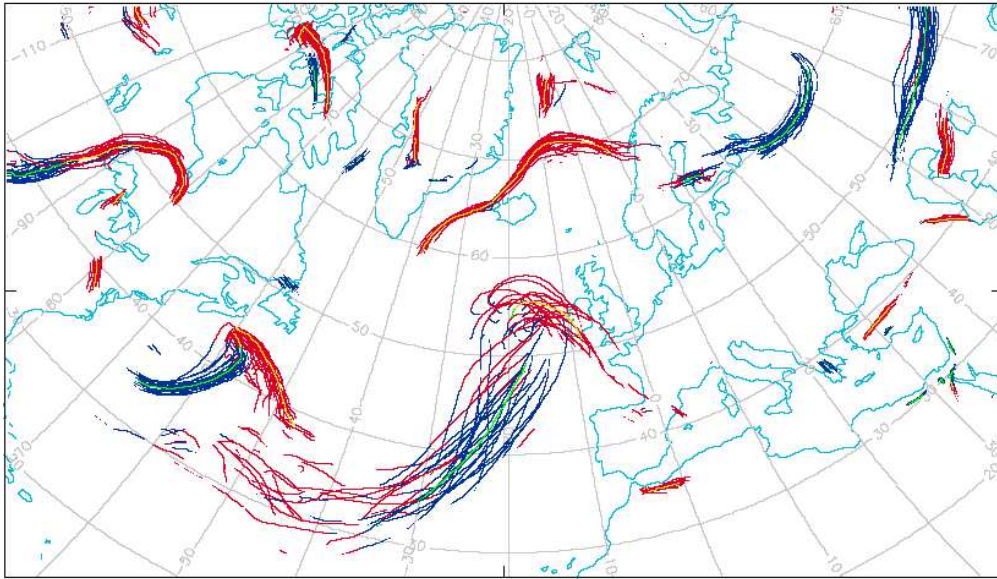


Figure 8: Composite "spaghetti" plot of fronts identified in all 24 MOGREPS-15 ensemble members for the T+36h forecast from DT 0000 UTC 24 April 2008, taken from a multiple lead-time animation. Cold/warm fronts are shown in blue/red for perturbed members and green/gold for the control forecast. Thermally weak fronts are omitted. Note the large spread in handling of features to the west and southwest of the UK, and relatively small spread for all other features.  
288x171mm (72 x 72 DPI)

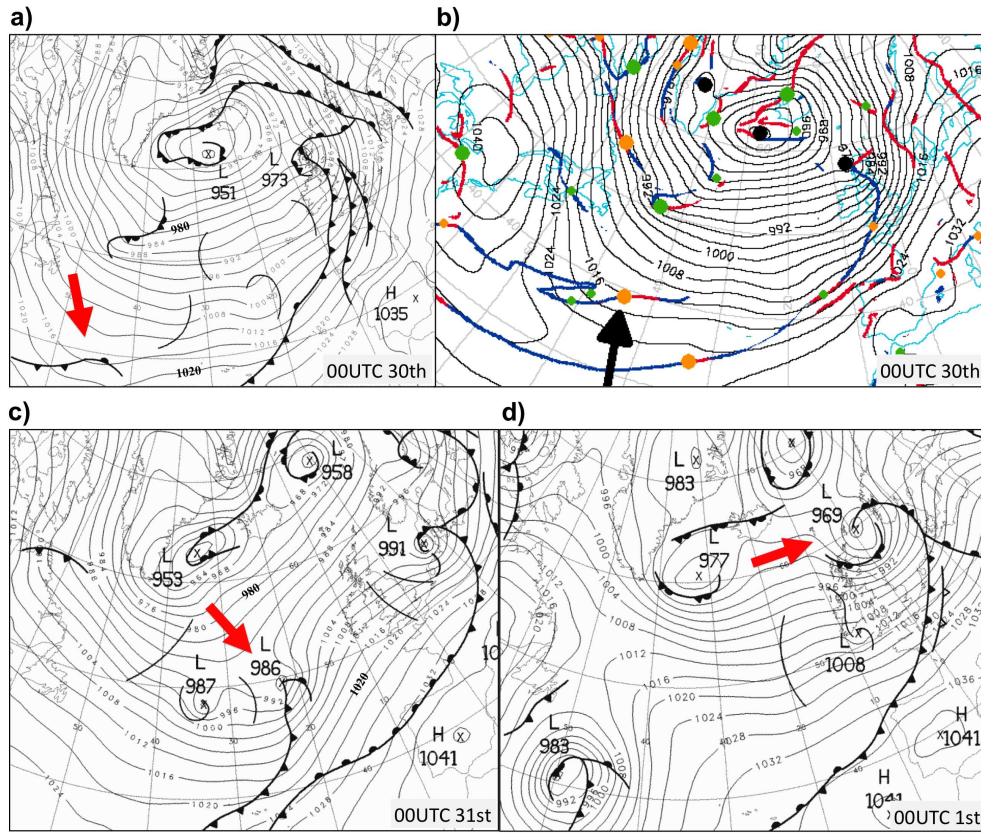


Figure 9: Manually-analysed synoptic charts from the Met Office for 0000 UTC on 30th (a), and 31st (c) December 2006, and 1st January 2007 (d). Objectively identified fronts and cyclonic features in the MOGREPS control analysis for 0000 UTC 30th are shown in (b) - see Figure 2 for symbol meaning. Isobar interval on all panels is 4hPa. Arrows highlight the developing cyclone discussed in the text. In the web version of panel (b) the user can click on any feature spot to bring up feature-specific information such as that shown on Figure 10.

930x777mm (72 x 72 DPI)

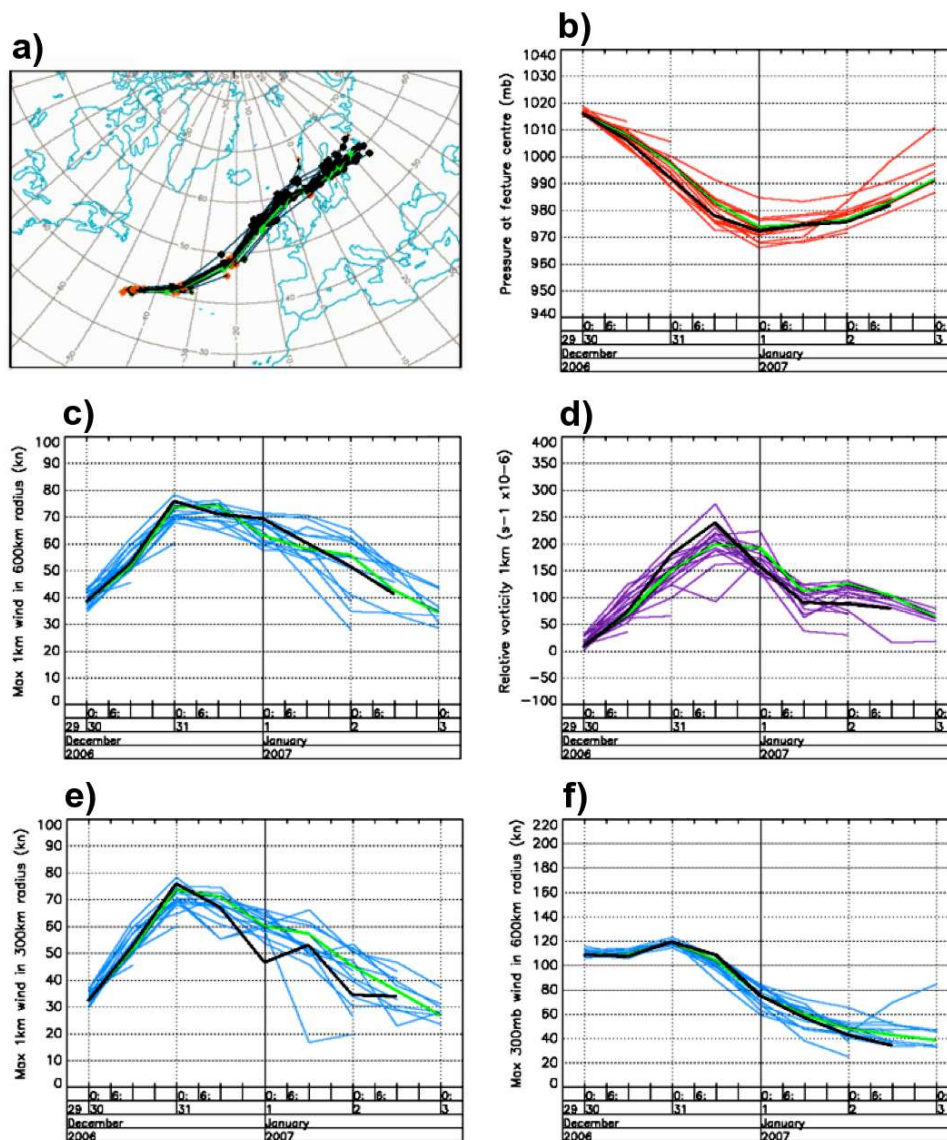


Figure 10: MOGREPS-15 ensemble: a) Forecast tracks for the key frontal wave from 0000 UTC 30 December 2006 (arrowed on Figure 9b). b)-f) Associated feature-specific plumes for five diagnostic measures (control=green, analysis=black). Vertical lines denote 0000 UTC on consecutive days, year change is darker. b) mean sea level pressure at the feature point (hPa), c) maximum 1 km wind within 600 km of the feature point (knots), d) relative vorticity at the feature point ( $\times 10^{-6} \text{ s}^{-1}$ ), e) maximum 1 km wind within 300 km of the feature point (knots). f) maximum 300 hPa wind within 600 km of the feature point (knots). Tabulated data that shows, as a function of lead, the percentage of members that captured the feature, have been omitted.

388x451mm (72 x 72 DPI)

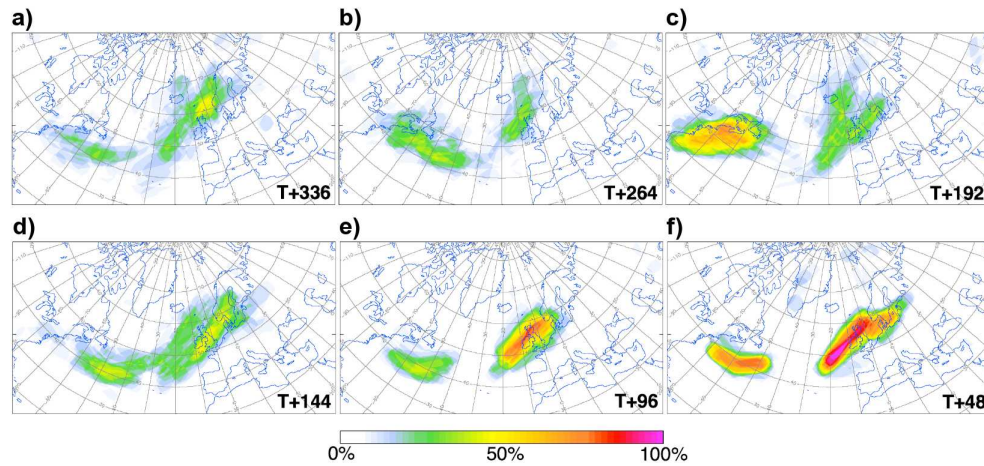


Figure 11: MORGREPS-15 ensemble 'storm track strike probability' forecasts, from a range of lead times, for a fixed validity period of 0000-2400UTC on 31 December 2006. Colours show the probability that a cyclonic feature, that has attributed to it (i.e. within a 300km radius) a maximum 1 km wind of > 60 knots, will pass within 300 km during the 24 h period. Each panel denotes a different lead time: a) 336h, b) 264h, c) 192h, d) 144h, e) 96h, f) 48h.  
587x274mm (72 x 72 DPI)

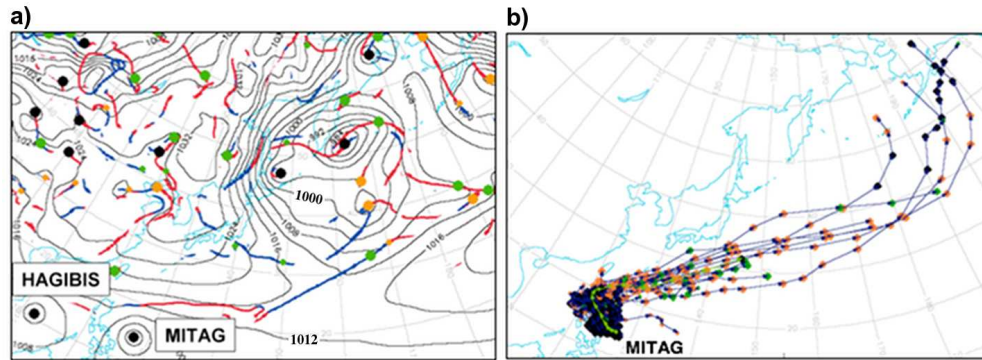


Figure 12: a): Objectively analysed fronts and features in the MOGREPS control analysis for 1200 UTC on 22 Nov 2007 (see Figure 2 for symbol meaning). Mean sea level pressure contours are at 4 hPa intervals. Two tropical cyclones have been identified: Hagibis in the South China Sea, and Mitag to the east of the Philippines. b) Forecast tracks for Typhoon Mitag from the same data time from the MOGREPS-15 ensemble. The storm was forecast to track over the Philippines, where it led to at least 10 fatalities, before undergoing extra-tropical transition. In the ensemble the acquisition of a frontal structure and the concurrent transition to the frontal wave cyclone class is denoted by a change from black to orange spots, and is evidently picked out well by the identification methods. This transition looks to occur in most members just after the completion of recurvature.

508x183mm (72 x 72 DPI)

1  
2  
3  
4  
5  
6  
7  
8  
9  
10  
11  
12  
13  
14  
15  
16  
17  
18  
19  
20  
21  
22  
23  
24  
25  
26  
27  
28  
29  
30  
31  
32  
33  
34  
35  
36  
37  
38  
39  
40  
41  
42  
43  
44  
45  
46  
47  
48  
49  
50  
51  
52  
53  
54  
55  
56  
57  
58  
59  
60

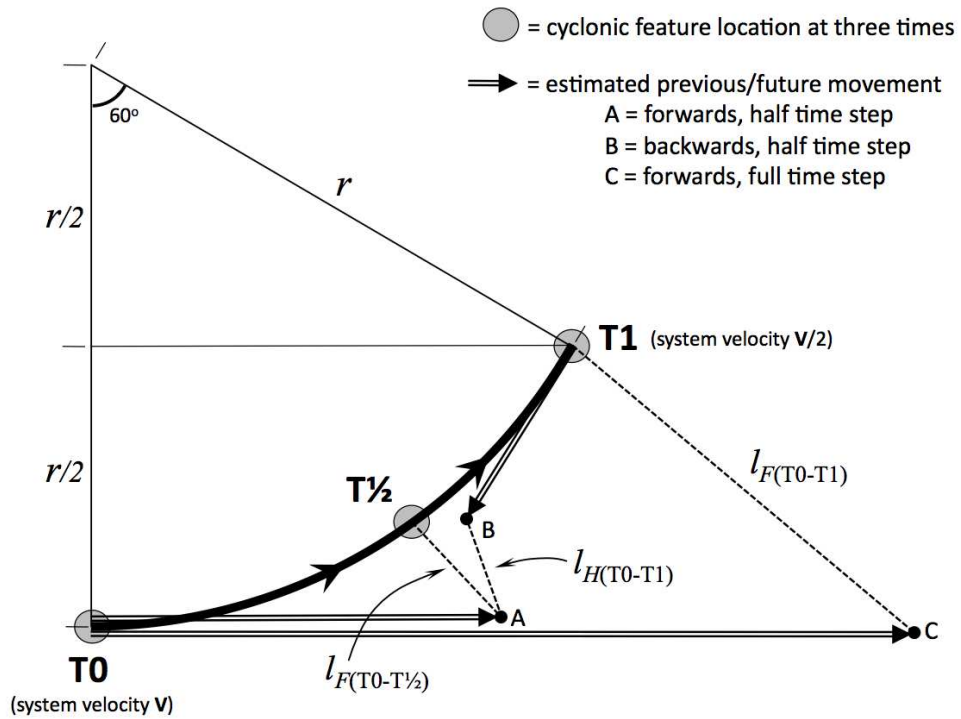


Figure A1: Idealized case of a cyclonic feature 'turning to the left', along the arc of a circle of radius  $r$ , linearly reducing its speed by 50% in  $60^\circ$ . Grey spots denote feature position at three equally spaced times. Distances  $l_{H(t)}$  and  $l_{F(t)}$  denote, respectively, the association errors for half-time tracking and full-time tracking of that feature, for frame time interval  $t$ . The figure is essentially drawn to scale, albeit with some arrows offset slightly to aid clarity.  
409x305mm (72 x 72 DPI)